Lifetime measurements and terminating structures in ^{87}Nb

J. Pavan,[1] S. L. Tabor,[1] A. V. Afanasjev,[2,3] C. Baktash,[4] F. Cristancho,[5] M. Devlin,[6] J. Döring,[2,*] C. J. Gross,[7] G. D. Johns,[8] R. A. Kaye,[1,†] D. R. LaFosse,[6] I. Y. Lee,[9] F. Lerma,[6] A. O. Macchiavelli,[9] I. Ragnarsson,[10] D. G. Sarantites,[6] and G. N. Solomon[1]

[1]*Department of Physics, Florida State University, Tallahassee, Florida 32306*
[2]*Department of Physics, University of Notre Dame, Notre Dame, Indiana 46556*
[3]*Laboratory of Radiation Physics, Institute of Solid State Physics, University of Latvia, LV-1063 Riga, Latvia*
[4]*Physics Division, Oak Ridge National Laboratory, Oak Ridge, Tennessee 37831*
[5]*Departmento de Física, Universidad Nacional de Colombia, Bogotá, Colombia*
[6]*Chemistry Department, Washington University, St. Louis, Missouri 63130*
[7]*UNISOR, Oak Ridge Institute of Science and Education, Oak Ridge, Tennessee 37831*
[8]*Los Alamos National Laboratory, Los Alamos, New Mexico 87545*
[9]*Nuclear Science Division, Lawrence Berkeley National Laboratory, Berkeley, California 94720*
[10]*Department of Mathematical Physics, Lund Institute of Technology, S-21100 Lund, Sweden*

(Received 23 September 2002; published 25 March 2003)

Two experiments have been performed using the ^{58}Ni(^{32}S,3p) reaction at 135 MeV with Gammasphere and the Microball to study the high-spin structure of the transitional nucleus ^{87}Nb. The first experiment using a thin target provided a considerable extension and refinement of the level scheme, as well as firm spin assignments from directional correlation of oriented nuclei. Sub-picosecond lifetimes were measured in the second backed-target experiment using the Doppler-shift attenuation method. The lifetimes imply a rather modest average deformation of $\beta_2 \sim 0.1$, but with considerable variation from state to state. Strong alternations were observed in the $B(M1)$ strengths of transitions between some pairs of bands. The experimental results were compared with calculations performed within the cranked Nilsson-Strutinsky approach. The calculations generally reproduce the irregularities in the structure of the yrast lines and plunging transition quadrupole moments Q_t within the bands explaining them as reflections of configuration changes and an approach of band termination, respectively.

DOI: 10.1103/PhysRevC.67.034316 PACS number(s): 21.10.Tg, 27.50.+e, 21.10.Ky, 21.60.Ev

I. INTRODUCTION

Transitional nuclei, which lie between those with spherical and highly deformed shapes, can provide valuable insights into the interplay between single-particle and collective degrees of freedom and present some interesting theoretical challenges. In the f-p-g shell, such a region lies around the neutron numbers N of 45 and 46. For smaller N, nearer to the middle of the shell, mean field models such as the cranked Hartree-Fock-Bogolyubov (CHFB) calculations have worked relatively well, while limited-basis shell-model calculations have generally been more successful near $N=50$.

The $N=45$ nucleus ^{86}Nb exhibits a rather well-defined band structure [1], although the CHFB calculations predict mainly spherical and superdeformed shapes. Lifetime measurements [2] indicate quadrupole deformations β_2 around 0.2. Deformations in the yrast positive-parity band decrease from $\beta_2 \approx 0.27$ to 0.10 as the spin increases from $8\hbar$ to $16\hbar$. This decrease, which does not correspond to the behavior of the moments of inertia, awaits theoretical understanding. There is a shallow oblate minimum in some of the total Routhian surfaces (TRS) of the CHFB calculations around $\beta_2 \approx 0.2$, but it does not vary systematically with spin. Somewhat a less regular and more complex band structure is seen in the $N=46$ isobar ^{86}Zr [3], suggesting that even the addition of one neutron significantly reduces the collectivity. The irregularities in the energy level structure of ^{86}Zr are reproduced quite well by calculations within the configuration-dependent shell-correction approach using a cranked Nilsson potential [cranked Nilsson-Strutinsky (CNS) approach]. These calculations explicitly connect the observed irregularities with the underlying single-particle structure of the f-p-g shell (band terminations).

The energy level scheme of $N=46$ ^{87}Nb [4,5] resembles that of the $N=46$ isotone ^{86}Zr more than the $Z=41$ isotope ^{86}Nb. That is, the addition of one more neutron leads to a band structure in ^{87}Nb which is more complex and less regular than in ^{86}Nb. Recoil-distance lifetime measurements [4] show a wide range of $B(E2)$ strengths from about 45 Weisskopf units (W.u.) among the low-lying positive-parity states to 2–8 W.u. among the low-lying negative-parity states. A direct timing measurement [6] yielded an even smaller value of $B(E2)=0.21$ W.u. for the lowest $\frac{5}{2}^- \rightarrow \frac{1}{2}^-$ transition. Above the first change in structure, the $B(E2)$ strengths drop to 10–15 W.u. in the positive-parity band but increase to 14–45 W.u. in the negative-parity band. In addition to all these variations in deformation and collectivity, four superdeformed bands have been seen at higher excitation energies [7]. A number of measurements [8–12] have been made for g factors in ^{87}Nb to provide more information on the single-

*Present address: GSI, 64291 Darmstadt, Germany.

†Present address: Department of Chemistry and Physics, Purdue University Calumet, Hammond, IN 46323.

particle structure. Shell-model calculations in the limited $(g_{9/2}, p_{1/2})$ space with Gross and Frenkel or surface-δ two-body matrix elements have not been as successful in explaining the electromagnetic properties or lower level scheme for ^{87}Nb as with $47 \leqslant N$ nuclei. An expanded model space or collective degrees of freedom appear to be needed [6,13,14].

Thus, the transition between collective and single-particle structure peaks at neutron number 46 in the $A \approx 80$ region. Although the competition between collective and single-particle excitations appears fragile and almost chaotic, the positive-parity band structures of the odd Z, $N=46$ isotones ^{83}Rb, ^{85}Y, ^{87}Nb, and ^{89}Tc are quite similar [15], indicating that the level schemes are considerably more robust than might be thought. The principal goal of the present work was to explore the evolution of band structure and collectivity in ^{87}Nb to higher spins in order to provide further insight into the $N=46$ transitional region and the effects of the underlying single-particle structure. Sub-picosecond lifetimes were determined using the Doppler-shifted attenuation method (DSAM) from γ-ray line shapes measured by using GAMMASPHERE and the MICROBALL. An examination of earlier thin-target data to determine the side-feeding intensities also led to a significant extension of the level scheme and the assignment of spins using the directional correlation of oriented (DCO) nuclei.

II. EXPERIMENTAL TECHNIQUE

For both experiments, high-spin states in ^{87}Nb were populated using the ^{58}Ni(^{32}S,$3p$) reaction with 135 MeV beams from the 88 Inch Cyclotron at Lawrence Berkeley National Laboratory. The evaporated charged particles were detected with the MICROBALL [16], an array of 95 CsI (Tl) scintillators covering 97% of the full sphere. γ rays from the reaction were detected using GAMMASPHERE [17].

In the first experiment, a 245 μg/cm^2 self-supporting ^{58}Ni foil enriched to 99.7% was used. 4.2×10^8 events with three or more γ rays were recorded using the early implementation of GAMMASPHERE with 36 Compton-suppressed high purity germanium (HPGe) detectors.

A target consisting of 415 μg/cm^2 of highly enriched ^{58}Ni evaporated onto a 10.3 mg/cm^2 Ta backing was used for the second experiment to measure lifetimes with the DSAM. The beam current was about 3.5 particle nA. GAMMASPHERE contained 95 HPGe detectors during this experiment.

III. ANALYSIS TECHNIQUE

A. Thin-target experiment

Data from the thin-target experiment, which has already yielded a rich harvest of physics [3,7,18–20], were first analyzed with in-house software to determine the decay intensity pattern for side-feeding corrections and to see what contributions the additional statistics provided by GAMMASPHERE could make to the level scheme. Energy and efficiency calibrations were made in the standard manner [1], and a Doppler-shift corrected $E_\gamma - E_\gamma$ matrix was constructed in coincidence with the detection of two or three protons in the MICROBALL. Four-proton coincidences were subtracted out of the matrix to remove contamination from the very strong ^{86}Zr channel. A portion of the particle-gated γ spectrum in coincidence with individual γ lines in the negative-parity bands is shown in the top panel of Fig. 1.

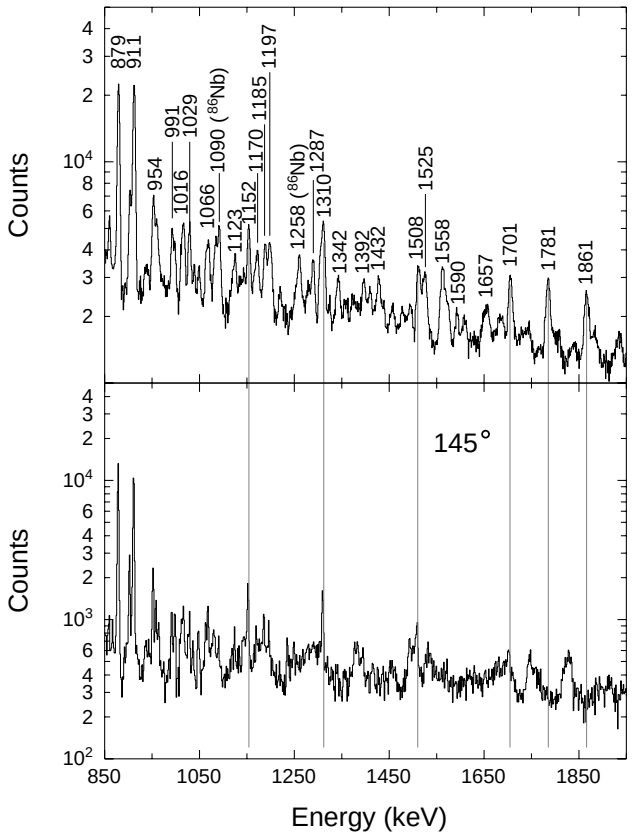

FIG. 1. A comparison of the γ spectra from the thin (top) and backed (bottom)-target experiments. Both spectra are gated on the condition of two or three protons with a portion of the four-proton coincidences subtracted. The top spectrum is summed over all early implementation γ detectors after Doppler-shift correction and also requires a coincident γ line at 136, 169, 264, 268, 298, 314, 506, 582, 807, 879, or 911 keV. The bottom spectrum shows only the 145° detectors without any Doppler-shift correction and requires coincidences with pairs of the γ lines listed above at any angle.

All the coincidences implied by the previous level scheme [4] were observed. The improved statistics did show additional coincidences leading to some rearrangement of the level scheme, as shown in Fig. 2. An example is shown in Fig. 3, a portion of the γ spectrum in coincidence with the 1861 keV line in band 3. Coincidences are seen with the 1558, 1701, and 1781 keV transitions, although the prior level scheme [4] implies coincidences only with the 1701 and 1781 keV lines. Additional coincidences with the 1558 keV γ ray, such as the 1525, 1287, and 1203 keV lines resulted in a restructuring of the level scheme to include an additional band on the negative-parity side (band 3 in Fig. 2). In addition, γ rays were found extending band 1 to $(\frac{55}{2}^-)$, band 4 to $(\frac{55}{2}^-)$, band 8 to $(\frac{53}{2}^+)$, band 12 to $(\frac{59}{2}^+)$, and band 13 to $(\frac{41}{2}^+)$. Also, many more intraband $M1$ transitions were discovered. Additionally, the sequence of the 959 and

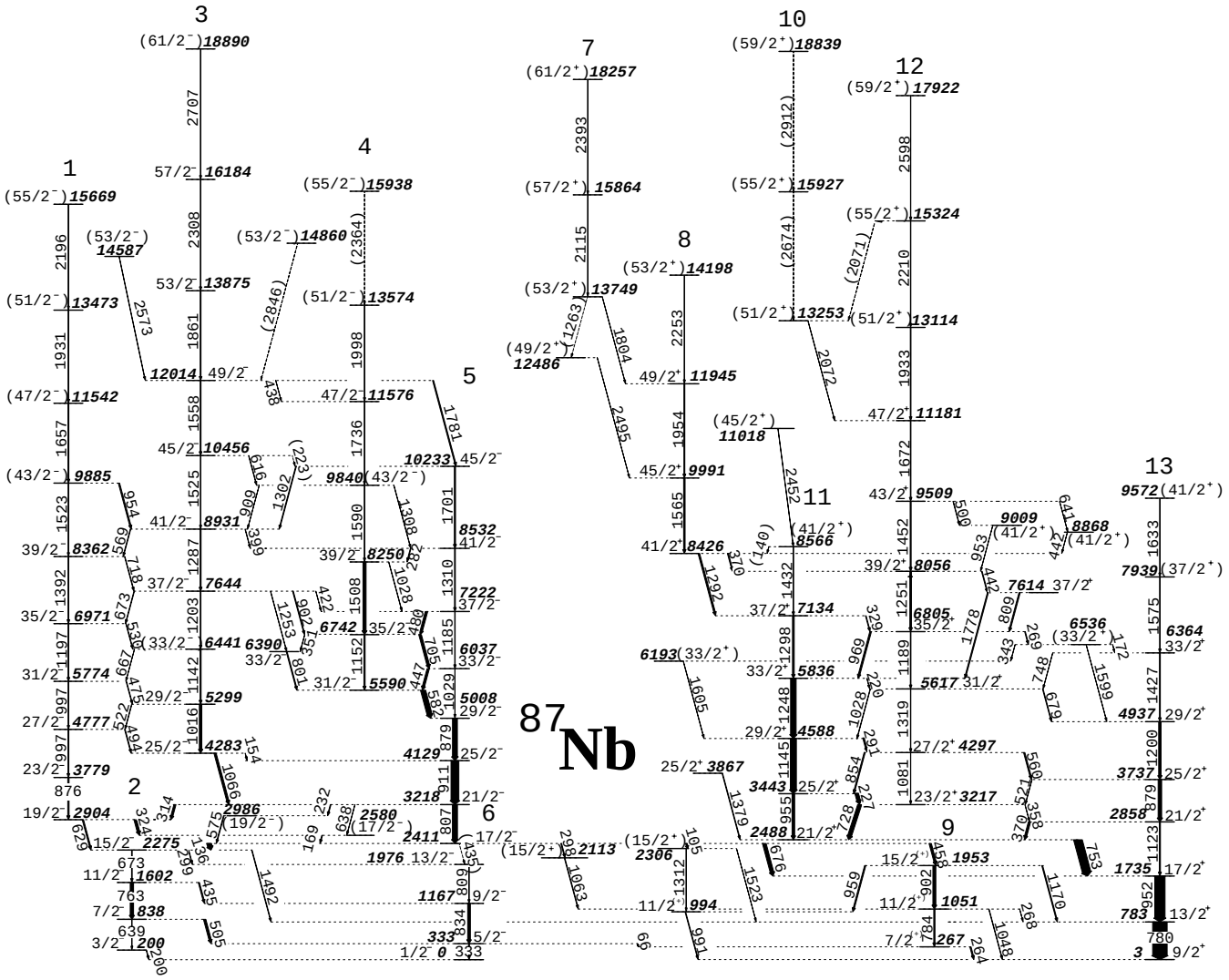

FIG. 2. The level scheme for ^{87}Nb deduced from the present work. Some spin assignments for low-lying transitions have been taken from previous work [4].

991 keV lines was inverted as compared to a previous work [4], and this is supported by many linking transitions. Finally, bands 7 and 10 were found and placed in the level scheme.

The same matrix was used to determine the relative intensities of the γ rays in ^{87}Nb to help correct the lifetime measurements from the backed-target experiment for feeding. In addition, another matrix was made by sorting the γ rays detected in the six detectors at 90° against the detectors placed at 17.275°, 37.38°, 142.62°, and 162.725° in order to determine the DCO ratios for as many transitions as possible. For this geometry and the gates used on stretched $E2$ decays, a DCO ratio of 1.0 is expected for electric quadrupole ($E2$) transitions and a DCO ratio between 0.35 and 0.55 is expected for dipole transitions ($M1$ and $E1$) with a small mixing ratio [21]. Using this matrix, the spins and parities of states up to $\frac{57}{2}^-$ and $\frac{49}{2}^+$ were deduced. The spins for states above these were tentatively assigned assuming stretched $E2$ transitions. The DCO ratios and intensities determined in the present work are summarized in Table I.

B. Doppler-Shift attenuation method lifetime analysis

After particle identification with in-house software, the data from the backed target were sorted by particle channel and transferred to disk to facilitate multiple sorts. All the γ-γ matrices were sorted on the condition of two or three detected protons, with subtraction of the four-proton channel. Also, the 1α-$2p$ channel was subtracted from the matrices used to analyze the positive-parity bands to remove contamination from ^{84}Zr. These subtractions approximately compensated for the cases where either one proton or one α was not detected. A third γ ray, any of the lower, unshifted transitions in the band of interest, was also required as a gate on the matrices. For comparison with the thin-target data, the same portion of the particle-gated γ spectrum at 145° in coincidence with pairs of γ lines in the negative-parity bands is shown in the lower panel of Fig. 1. The higher-energy γ lines generally show more Doppler shifting than do the lower-energy ones.

In order to perform DSAM measurements, each square matrix consisted of data from all detectors on one axis and

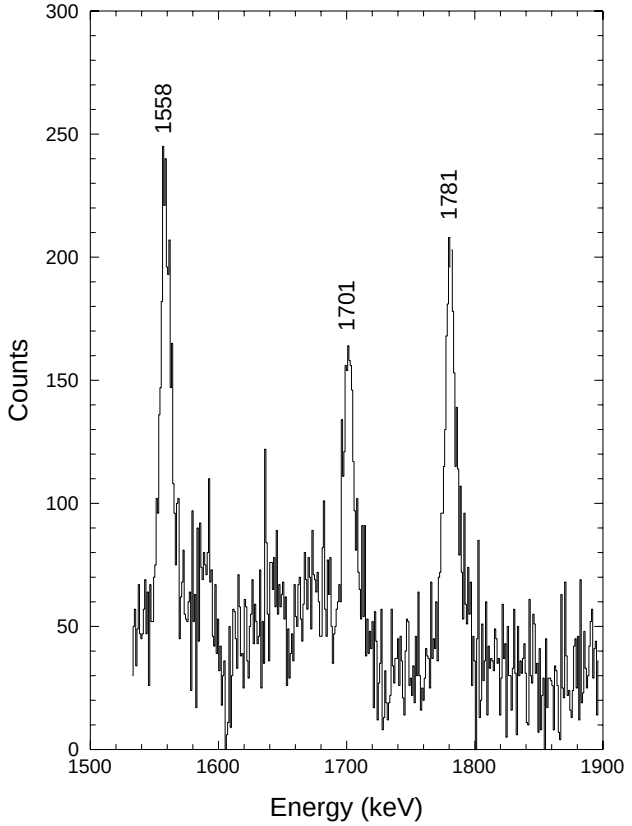

FIG. 3. A portion of the spectrum in coincidence with the 1861 keV line in band 3.

data from detectors at a specific angle on the other. In this case, we combined the detectors in the rings at 31.717° and 37.377° for a set of detectors at an effective angle of 34.95°, used the rings of detectors at 50.065° and 129.934°, and combined the detectors at 142.622° and 148.282° for an effective angle of 145.45°. In cases when statistics were poor, we also added the detectors at 58.282° to those at 50.065° for a ring at an effective angle of 52.80° and added the detectors at 121.717° to those at 129.935° for a set of detectors at 127.20°. Figure 4 shows the line shapes of the 1781 keV γ ray at 34.95°, 50.065°, 129.934°, and 145.45°. As was shown in a prior work [2], the difference between the sums of simulations for the line shapes of nearby angles and a single line shape calculated at the effective angle is well within the statistical uncertainties in the data.

Line shapes were obtained by placing an additional gate on the axis of the square matrix containing all the detectors. Thus, all the line shapes analyzed were gated first by particle channel and then by two γ gates. Often spectra gated on several different transitions were added to improve statistics. One set of matrices was constructed without any Doppler-shift corrections. Line shapes were extracted from these matrices by gating on lines which show little or no Doppler shifting, i.e., below the line shapes of interest. In addition, other sets of γ-γ matrices were constructed by approximately correcting for Doppler shifting on the axis containing all the detectors. The spectra were shifted to compensate for velocities $\beta(=v/c)$, somewhat less than the initial recoil

TABLE I. A summary of DCO ratios and intensities determined using the thin-target data.

E_x (keV)	I_i^π	E_γ (keV)	Intensity	R_{DCO}
18890	$(\frac{61}{2}^-)$	2706.8	1.5±0.8	
18839	$(\frac{59}{2}^+)$	(2912)		
18257	$(\frac{61}{2}^+)$	2392.9	0.5±0.3	$0.90^{+0.10}_{-0.09}$
17922	$(\frac{59}{2}^+)$	2598.4	2.3±0.5	$0.95^{+0.16}_{-0.14}$
16184	$\frac{57}{2}^-$	2308.4	3.1±0.6	
15938	$(\frac{55}{2}^-)$	(2364)		
15927	$(\frac{55}{2}^+)$	(2674.0)		
15864	$(\frac{57}{2}^+)$	2114.7		
15669	$(\frac{55}{2}^-)$	2196.0	1.4±0.7	
15324	$(\frac{55}{2}^+)$	2209.6	2.7±0.9	
		(2071)		
14860	$(\frac{53}{2}^-)$	(2846)		
14587	$(\frac{53}{2}^-)$	2573.0	1.9±0.9	
14198	$(\frac{53}{2}^+)$	2253.1	1.3±0.6	
13875	$\frac{53}{2}^-$	1861.2	5.7±0.6	$0.98^{+0.09}_{-0.08}$
13749	$(\frac{53}{2}^+)$	1804.1	0.8±0.4	
		(1263)		
13574	$(\frac{51}{2}^-)$	1998.1	2.3±1.0	
13473	$(\frac{51}{2}^-)$	1931.0	3.9±0.4	
13253	$(\frac{51}{2}^+)$	2072.0	1.4±0.7	
13114	$(\frac{51}{2}^+)$	1933.0	4.8±0.5	
12486	$(\frac{49}{2}^+)$	2495.1	0.3±0.2	
12014	$\frac{49}{2}^-$	1780.8	7.3±0.7	$1.19^{+0.25}_{-0.21}$
		1557.6	5.8±0.6	$0.93^{+0.11}_{-0.10}$
		437.6		$0.48^{+0.12}_{-0.10}$
11945	$\frac{49}{2}^+$	1954.3	6.3±0.6	$1.04^{+0.07}_{-0.07}$
11576	$\frac{47}{2}^-$	1736.3	2.4±0.8	
11542	$(\frac{47}{2}^-)$	1656.7	6.1±0.6	
11181	$\frac{47}{2}^+$	1672.4	4.4±0.4	$1.01^{+0.06}_{-0.06}$
11018	$(\frac{45}{2}^+)$	2452.3	1.4±0.5	
10456	$\frac{45}{2}^-$	1525.1	1.8±0.9	$0.95^{+0.13}_{-0.12}$
		616.3	2.6±0.4	
		223		
10233	$\frac{45}{2}^-$	1701.2	8.2±0.8	$0.84^{+0.12}_{-0.10}$
		1301.9	4.8±1.0	
9991	$\frac{45}{2}^+$	1565.1	10.1±1.0	$1.03^{+0.04}_{-0.04}$
9885	$(\frac{43}{2}^-)$	1522.7	2.4±0.6	
		953.8	8.9±2.7	
9840	$(\frac{43}{2}^-)$	1590.1	2.8±0.6	
		1308.1	1.7±0.6	
		908.8		
9572	$(\frac{41}{2}^+)$	1633.0	2.0±0.6	
9509	$\frac{43}{2}^+$	1452.3	7.0±0.7	$1.10^{+0.05}_{-0.05}$
		641.1	0.9±0.5	
		499.6	2.8±0.6	
9009	$(\frac{41}{2}^+)$	952.7		

TABLE I. (*Continued*.)

E_s (keV)	I_i^π	E_y (kev)	Intensity	R_{DCO}
8931	$\frac{41}{2}^-$	1287.1	6.8±1.4	$1.20^{+0.25}_{-0.20}$
		568.9	3.8±0.4	$0.47^{+0.09}_{-0.08}$
		399.3	2.2±0.4	
8868	$(\frac{41}{2}^+)$	441.6	0.5±0.3	
8566	$(\frac{41}{2}^+)$	1431.8	3.4±0.7	
		(140)		
8532	$\frac{41}{2}^-$	1310.0	5.6±0.6	$0.74^{+0.08}_{-0.07}$
		282.0	4.3±0.4	$0.47^{+0.07}_{-0.06}$
8426	$\frac{41}{2}^+$	1291.5	10.9±1.1	$1.10^{+0.09}_{-0.03}$
		369.6	6.9±1.4	$0.58^{+0.03}_{-0.03}$
8362	$\frac{39}{2}^-$	1391.6	5.2±0.5	$1.02^{+0.18}_{-0.15}$
		718.2	3.1±0.6	
8250	$\frac{39}{2}^-$	1508.2	21.5±2.2	
		1028.0	1.8±0.8	$0.58^{+0.03}_{-0.03}$
8056	$\frac{39}{2}^+$	1251.2	10.9±2.2	
		442.3	4.8±0.5	$0.47^{+0.04}_{-0.04}$
7939	$(\frac{37}{2}^+)$	1575.0	4.0±0.8	
7644	$\frac{37}{2}^-$	1253.7	1.8±0.9	$0.94^{+0.08}_{-0.07}$
		1203.3	4.8±2.4	
		902.4	5.5±1.1	$0.64^{+0.13}_{-0.11}$
		673.4	3.3±0.7	
		422.2	0.9±0.5	$0.59^{+0.26}_{-0.26}$
7614	$\frac{37}{2}^+$	1777.7	6.9±0.7	$0.95^{+0.07}_{-0.07}$
		808.9	8.5±1.7	$0.55^{+0.05}_{-0.05}$
7222	$\frac{37}{2}^-$	1185.2	3.3±0.7	$0.99^{+0.06}_{-0.06}$
		480.2	16.5±1.7	$0.54^{+0.02}_{-0.02}$
7134	$\frac{37}{2}^+$	1298.1	11.7±2.3	$1.02^{+0.09}_{-0.08}$
		329.3	4.4±0.4	$0.52^{+0.04}_{-0.04}$
6971	$\frac{35}{2}^-$	1196.8	4.8±2.4	$0.99^{+0.05}_{-0.05}$
		529.9	3.2±0.3	
6805	$\frac{35}{2}^+$	1188.6	4.2±0.8	
		968.8	11.3±1.1	$0.62^{+0.07}_{-0.06}$
		269.1	4.7±0.9	$0.48^{+0.04}_{-0.04}$
6742	$\frac{35}{2}^-$	1151.8	8.3±0.8	$0.97^{+0.05}_{-0.05}$
		705.0	17.9±1.8	$0.51^{+0.02}_{-0.02}$
		351.3	4.0±0.4	$0.64^{+0.03}_{-0.03}$
6536	$(\frac{33}{2}^+)$	1598.7	0.9±0.5	
		342.7	1.0±0.5	
		172.0	1.4±1.0	
6441	$(\frac{33}{2}^-)$	1141.9	7.3±0.7	
		666.9	0.8±0.4	
6390	$\frac{33}{2}^-$	800.5	6.3±0.6	$0.58^{+0.03}_{-0.03}$
6364	$\frac{33}{2}^+$	1426.7	6.0±1.2	$1.00^{+0.29}_{-0.16}$
		747.5	0.9±0.5	
6193	$(\frac{33}{2}^+)$	1605.1	1.7±0.6	
6037	$\frac{33}{2}^-$	1028.8	1.6±0.6	$0.96^{+0.11}_{-0.10}$
		446.8	15.6±1.6	$0.57^{+0.02}_{-0.02}$
5836	$\frac{33}{2}^+$	1248.1	38.3±3.8	$0.99^{+0.05}_{-0.04}$
		219.8	1.8±0.6	$0.37^{+0.07}_{-0.06}$
5774	$\frac{31}{2}^-$	997.1	2.9±0.6	
		475.0	3.7±0.4	$0.74^{+0.08}_{-0.07}$

TABLE I. (*Continued*.)

E_s (keV)	I_i^π	E_y (kev)	Intensity	R_{DCO}
5617	$\frac{31}{2}^+$	1319.4	2.7±0.3	$1.04^{+0.05}_{-0.05}$
		1028.3	2.4±0.9	
		679.2	4.4±0.9	$0.46^{+0.04}_{-0.04}$
5590	$\frac{31}{2}^-$	582.0	34.9±3.5	$0.54^{+0.02}_{-0.02}$
5299	$\frac{29}{2}^-$	1015.9	17.0±1.7	$1.04^{+0.06}_{-0.06}$
		522.1	2.4±0.5	$0.32^{+0.21}_{-0.09}$
5008	$\frac{29}{2}^-$	879.3	33.7±6.7	$1.09^{+0.03}_{-0.03}$
4937	$\frac{29}{2}^+$	1200.1	16.7±3.3	$1.16^{+0.08}_{-0.07}$
4777	$\frac{27}{2}^-$	997.4	5.9±1.2	
		493.8	4.7±0.5	$0.87^{+0.31}_{-0.28}$
4588	$\frac{29}{2}^+$	1145.1	41.6±4.2	$1.03^{+0.05}_{-0.05}$
		291.1	10.2±1.0	$0.55^{+0.05}_{-0.05}$
4297	$\frac{27}{2}^+$	1080.5	1.8±0.4	$0.95^{+0.05}_{-0.05}$
		854.0	7.7±0.8	$0.46^{+0.03}_{-0.03}$
		559.9	8.9±0.9	$0.49^{+0.03}_{-0.03}$
4283	$\frac{25}{2}^-$	1065.5	15.2±1.5	$1.22^{+0.11}_{-0.10}$
		154.4	1.2±1.1	$0.38^{+0.08}_{-0.07}$
4129	$\frac{25}{2}^-$	911.1	54.0±5.4	$0.96^{+0.03}_{-0.03}$
3867	$\frac{25}{2}^+$	1378.7	4.1±0.4	$1.11^{+0.09}_{-0.08}$
3779	$\frac{23}{2}^-$	875.5	9.0±8.0	$1.00^{+0.01}_{-0.11}$
3737	$\frac{25}{2}^+$	878.7	24.3±2.4	$0.88^{+0.07}_{-0.06}$
		520.6	1.8±0.9	$0.51^{+0.04}_{-0.04}$
3443	$\frac{25}{2}^+$	954.8	17.9±3.6	$0.94^{+0.02}_{-0.02}$
		226.5	23.5±2.4	$0.47^{+0.02}_{-0.02}$
3218	$\frac{21}{2}^-$	806.5	34.9±7.0	$0.95^{+0.03}_{-0.03}$
		637.9	1.4±0.7	$0.62^{+0.03}_{-0.03}$
		313.6	14.2±1.4	$0.51^{+0.03}_{-0.03}$
		231.5	4.9±0.8	$0.82^{+0.27}_{-0.27}$
3217	$\frac{23}{2}^+$	728.3	27.4±2.7	$0.49^{+0.02}_{-0.02}$
		358.1	1.7±0.6	
2986	$(\frac{19}{2}^-)$	575.0	4.4±0.4	
2904	$\frac{19}{2}^-$	628.9	9.0±1.8	$1.05^{+0.10}_{-0.09}$
		324.4	17.9±1.8	$0.46^{+0.02}_{-0.02}$
2858	$\frac{21}{2}^+$	1123.2	7.8±0.8	$0.99^{+0.07}_{-0.07}$
		370.2	15.2±1.5	$0.60^{+0.03}_{-0.03}$
2580	$(\frac{17}{2}^-)$	168.6	5.0±1.0	$1.10^{+0.12}_{-0.12}$
2488	$\frac{21}{2}^+$	753.0	58.5±5.8	$1.09^{+0.03}_{-0.03}$
2411	$\frac{17}{2}^-$	675.7	24.9±5.0	$1.08^{+0.11}_{-0.10}$
		458.0	15.8±1.6	$0.59^{+0.03}_{-0.03}$
		(435)		
		297.9	5.4±1.1	$0.65^{+0.03}_{-0.03}$
		136.0	29.6±7.2	$0.50^{+0.16}_{-0.13}$
		104.6		
2306	$(\frac{15}{2}^+)$	1523.4		
		1312.4		
2275	$\frac{15}{2}^-$	1492.0	3.5±0.4	$0.52^{+0.07}_{-0.16}$
		673.3	4.4±0.9	$0.97^{+0.05}_{-0.04}$
		299.4	3.4±0.7	$0.59^{+0.04}_{-0.09}$
2113	$(\frac{15}{2}^+)$	1062.5	4.0±0.4	$0.62^{+0.09}_{-0.08}$
1976	$\frac{13}{2}^-$	808.5	2.0±0.6	

TABLE I. (*Continued*.)

E_s (keV)	I_i^π	E_y (kev)	Intensity	R_{DCO}
1953	$\frac{15}{2}^{(+)}$	1170.0	6.4±0.6	$0.58^{+0.05}_{-0.05}$
		959.0	8.6±1.8	$0.99^{+0.15}_{-0.13}$
		902.4	20.4±2.0	$0.87^{+0.08}_{-0.08}$
1735	$\frac{17}{2}^{+}$	952.3	71.2±14.2	$1.02^{+0.03}_{-0.02}$
1602	$\frac{11}{2}^{-}$	763.3	23.1±2.3	$1.05^{+0.07}_{-0.06}$
		434.6	8.2±0.8	$0.82^{+0.04}_{-0.04}$
1167	$\frac{9}{2}^{-}$	834.1	18.8±1.9	$0.97^{+0.03}_{-0.03}$
1051	$\frac{11}{2}^{(+)}$	1047.5	2.7±0.5	$1.16^{+0.20}_{-0.17}$
		783.6	8.3±2.6	$0.88^{+0.09}_{-0.08}$
		267.6		
994	$\frac{11}{2}^{(+)}$	990.9	4.3±0.4	$0.90^{+0.01}_{-0.01}$
838	$\frac{7}{2}^{-}$	638.8		
		505.4	16.1±1.6	$0.62^{+0.03}_{-0.03}$
783	$\frac{13}{2}^{+}$	779.9	100±10	$0.97^{+0.01}_{-0.01}$
333	$\frac{5}{2}^{-}$	333.0	5.8±0.6	$1.03^{+0.06}_{-0.06}$
		66.0		
267	$\frac{7}{2}^{(+)}$	263.9	8.4±0.8	$0.65^{+0.04}_{-0.04}$
200	$\frac{3}{2}^{-}$	199.6	3.0±0.6	$0.56^{+0.08}_{-0.07}$

value of $\beta \approx 0.035$ to allow for slowing down before the decays. No adjustments were ever made to the axis containing detectors at a single angle (or narrow range of angles), from which the line shapes were obtained. The second sorting method resulted in much sharper peaks in the total γ spectrum for short-lived states and made it possible to gate on transitions above the one whose line shape was being extracted. An example of the spectra corrected for several different values of β is shown in Fig. 5. The different ''focus'' obtained at different β values allowed for more selective gating. For example, the 1933.0 keV γ ray was selected by $\beta = 0.030$, while a $\beta = 0.025$ was better for the 1954.3 keV γ ray.

Lifetimes were determined by performing a least squares fit of the Doppler-shifted line shapes at each angle using the computer program FITS [22]. A best fit to the experimental line shape was determined by simulating the slowing down of decaying nuclei in the target and Ta backing. FITS simulates this process by integrating over the thickness of the target and backing in order to determine the distribution of recoil velocities as the nuclei slow down and decay. Stopping powers from SRIM 2000 were used [23]. Additionally, FITS can account for both feeding from higher states and side feeding from unknown states, when their lifetimes and relative intensities are known. We were able to account for feeding in all but the highest γ transitions studied.

First, effective lifetimes were determined for 31 states by averaging the results from fits to the line shapes at each of the four angles without any feeding corrections. Starting from the top, the effective lifetime of the highest state that could be measured was used to correct for direct feeding of the state below it. This process was then repeated down the band. The fraction of unobserved (or side) feeding was determined from the intensities measured in the thin-target experiment. The Doppler corrected matrices made it possible to

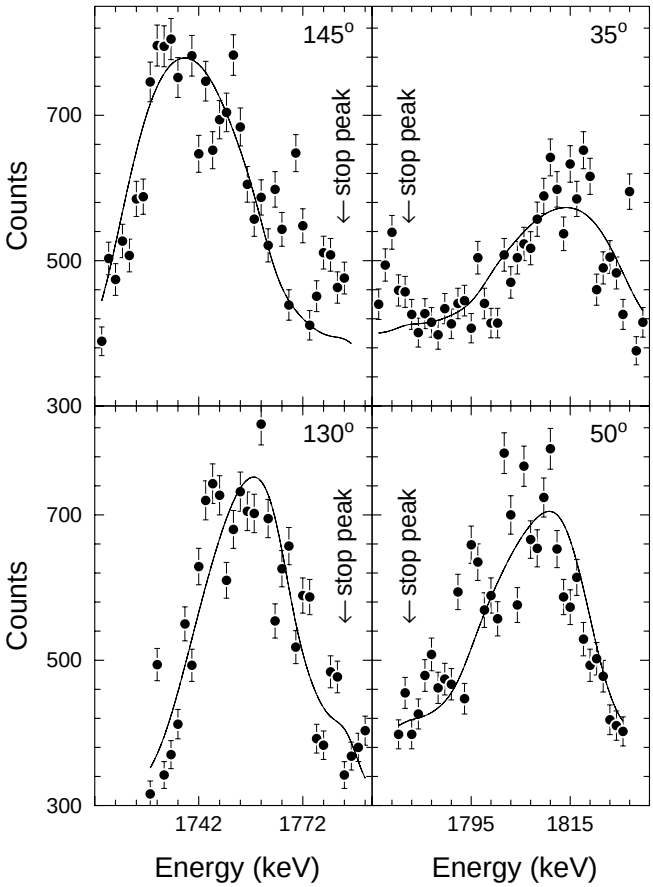

FIG. 4. The measured 1781 keV line shape from each of the angles 35°, 50°, 130°, and 145°. The best-fit simulations are shown as smooth curves.

place gates above the line shapes for the 1933.0 and 1452.3 keV γ rays in band 12, 1291.5 keV γ ray in band 8, 1298.1 and 1248.1 keV γ rays in band 11, and 1780.8 keV γ ray in band 5 to eliminate side feeding. In order to correct for side feeding in the states where gating from above was not possible, the side feeding times of the six aforementioned states were determined by a comparison of their gated from below line shapes with and without side feeding. From this information, we were able to establish a relationship between the effective lifetimes of each state and the side-feeding times of each state. Above 7330 keV the side feeding was determined to be 15% of the effective lifetime of the state and below 7330 keV the fraction of the effective lifetimes which corresponded to side feeding was determined by

$$\frac{\tau_{\rm sf}}{\tau_{\rm eff}} = -1.2\times10^{-4}E_x + 1.03, \tag{1}$$

where $\tau_{\rm eff}$ is in picoseconds and E_x is in keV. Feeding corrections generally improved the agreement between the measured line shapes and those simulated by FITS. The lifetimes of 31 states were determined and are summarized in Table II.

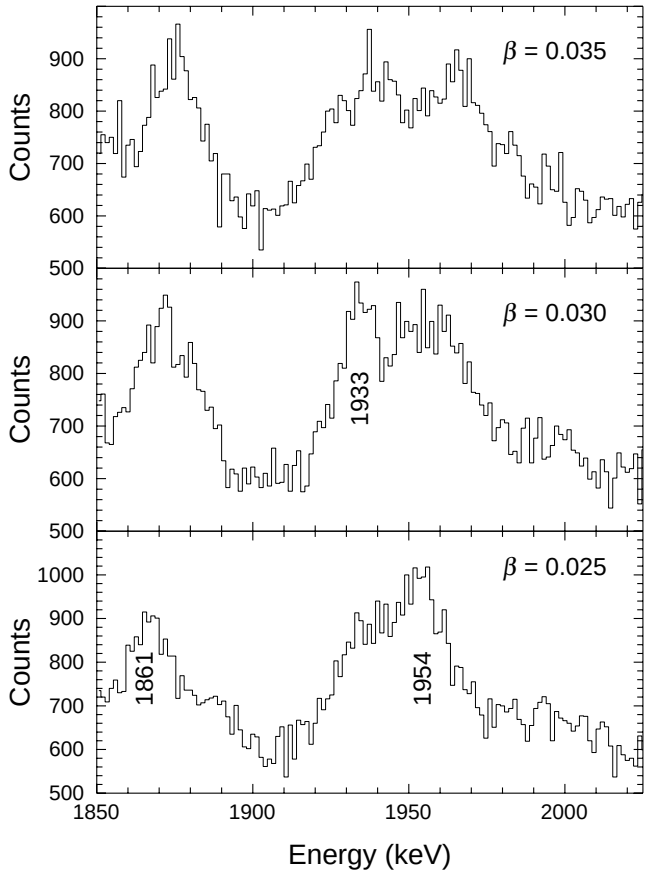

FIG. 5. A comparison of the γ spectra summed over all detectors after approximate correction for Doppler shifting from a source moving at the indicated velocities β (relative to the speed of light c).

The uncertainties in the lifetime measurements were determined by varying the lifetimes until the simulated line shapes generated by FITS were no longer consistent with the experimental data. The lifetimes at the individual angles were averaged by weighing with their uncertainties to determine the accepted lifetimes in the last column of Table II. The present DSAM measurements greatly extended the range of known lifetimes in ^{87}Nb, but did not overlap with prior recoil-distance lifetime measurements [4].

From the lifetimes in Table II and the transition energies and branching ratios from Table I, the quadrupole transition strengths and $B(E2)$ values were determined for the $\Delta I=2$ decays. Then the transition quadrupole moments Q_t were calculated according to the prescription

$$Q_t^2=\frac{16\pi}{5}\langle IK20|I-2K\rangle^{-2}B(E2,I\rightarrow I-2). \qquad (2)$$

These results are summarized in Table III. The magnetic dipole transition strengths $B(M1)$ were calculated for the $\Delta I=1$ decay assuming that the mixing ratios δ are zero. Small mixing ratios do not reduce the $B(M1)$ values significantly, and large mixing ratios tend to be rare in these nuclei. The $B(M1)$ values are listed in Table IV, and many are plotted in Fig. 6.

IV. DISCUSSION

The new level scheme shows that the bandlike structure in ^{87}Nb continues up in spin, with the same qualitative features seen at lower spins, such as irregularities in some energy spacings and band forkings. Sequences of states are observed whose energies increase with a constant moment of inertia, only to change abruptly to a significantly different moment of inertia. The measured lifetimes, when interpreted in a rotational model, would imply average quadrupole deformations of $\beta_2\sim 0.1$, although with considerable variation from state to state. In comparison, the band structure in ^{86}Nb is somewhat more regular, and the average quadrupole deformations are somewhat higher, with β_2 averaging closer to 0.2 [2]. This decreasing collectivity with increasing neutron number N is another indication of the transitional nature of these nuclei where even the addition of one neutron can change the average shape.

Due to the irregularities in band structure, there is some uncertainty in the grouping of levels in the bands in Fig. 2. The band groupings and labels are intended to facilitate the discussion. The energies of states in ^{87}Nb have been graphed as a function of spin in the middle panels of Figs. 7–10. In these graphs, the energies of a ''standard'' [24] rigid rotor $[E_{ld}=(\hbar^2/2J_{\rm rig})I(I+1)$ with $(\hbar^2)/2J_{\rm rig}=0.007\ (158/A)^{5/3}$ MeV$=18.9$ keV] have been subtracted to remove the dominant quadratic dependence on spin. As a result, bands with exactly the reference moment of inertia would form a horizontal line on these plots, and bands with a lower (higher) moment of inertia would form rising (falling) lines. The transition quadrupole moments Q_t inferred from the present and previous lifetime measurements are plotted in the bottom panels of Figs. 7–10.

A. Cranked Nilsson-Strutinsky (CNS) approach

In order to gain a better understanding of the structure of ^{87}Nb, calculations were performed within the configuration-dependent shell-correction approach using a cranked Nilsson potential (CNS approach) [25,26]. In CNS calculations, the configurations specified by the occupation of low-j and high-j orbitals with signatures α and approximate principle quantum numbers N_{shell} [26,27], are traced in the deformation $(\epsilon_2,\ \epsilon_4,\ \gamma)$ space as a function of spin I. The $A=80$ Nilsson potential parameters of Ref. [28] have been used in calculations. This approach neglects pairing correlations, so the calculations are realistic only for states with spins above $15\hbar$, and only these will be compared with experiment. Such an analysis has been successful in describing the high-spin terminating bands in other nuclei, including transitional ones such as nuclei around ^{62}Zn [29], ^{86}Zr [3], and ^{109}Sb [27,30,31]. Results of these calculations for the configurations that appear most relevant to the observed bands in ^{87}Nb are shown in the top panels of Figs. 7–10. The configurations of the dominant components of the bands shown in the

TABLE II. The lifetimes of 31 high-spin states, where only noted effective lifetimes could be determined because no feeding information was available for these states. The table includes the energies, spins, γ-ray energies, effective lifetimes, and corrected lifetimes, and is grouped by parity and signature.

E_x (keV)	I_i^π	E_γ (keV)	τ_{eff} (ps)	35°	50°	130°	145°	τ (ps)
				$\pi=+,\ \alpha=+\frac{1}{2}$				
11945	$\frac{49}{2}^+$	1954.3 [a]	$0.04^{+0.05}_{-0.03}$					
9991	$\frac{45}{2}^+$	1565.1	$0.50^{+0.07}_{-0.07}$	$0.28^{+0.13}_{-0.11}$	$0.17^{+0.11}_{-0.07}$	$0.36^{+0.06}_{-0.08}$	$0.35^{+0.07}_{-0.05}$	$0.32^{+0.05}_{-0.05}$
8426	$\frac{41}{2}^+$	1291.5	$1.04^{+0.08}_{-0.08}$	$0.55^{+0.08}_{-0.07}$	$0.61^{+0.07}_{-0.06}$	$0.57^{+0.11}_{-0.10}$	$0.68^{+0.14}_{-0.13}$	$0.58^{+0.09}_{-0.09}$
		369.6		$0.47^{+0.16}_{-0.11}$	$0.63^{+0.17}_{-0.13}$	$0.51^{+0.17}_{-0.12}$	$0.58^{+0.15}_{-0.12}$	
7134	$\frac{37}{2}^+$	1298.1	$1.54^{+0.14}_{-0.14}$	$0.34^{+0.08}_{-0.08}$	$0.35^{+0.07}_{-0.06}$	$0.50^{+0.07}_{-0.07}$	$0.45^{+0.10}_{-0.09}$	$0.43^{+0.06}_{-0.06}$
		329.3		$0.35^{+0.07}_{-0.07}$	$0.45^{+0.07}_{-0.06}$	$0.77^{+0.13}_{-0.12}$	$0.72^{+0.13}_{-0.11}$	
5828	$\frac{33}{2}^+$	1248.1 [b]		$0.40^{+0.22}_{-0.14}$	$0.33^{+0.21}_{-0.13}$	$0.50^{+0.26}_{-0.17}$	$0.75^{+0.53}_{-0.26}$	$0.42^{+0.13}_{-0.08}$
8566	$(\frac{41}{2}^+)$	1431.8	$1.02^{+0.10}_{-0.10}$	$1.08^{+0.48}_{-0.37}$	$0.91^{+0.30}_{-0.30}$	$0.68^{+0.57}_{-0.20}$	$0.95^{+0.46}_{-0.33}$	$0.92^{+0.20}_{-0.14}$
7614	$\frac{37}{2}^+$	1777.7	$1.01^{+0.10}_{-0.10}$	$0.22^{+0.22}_{-0.11}$	$0.54^{+0.17}_{-0.14}$	$0.59^{+0.31}_{-0.20}$	$0.55^{+0.19}_{-0.14}$	$0.48^{+0.10}_{-0.07}$
				$\pi=+,\ \alpha=-\frac{1}{2}$				
17922	$(\frac{59}{2}^+)$	2598.4 [a]	$0.04^{+0.09}_{-0.04}$					
15324	$(\frac{55}{2}^+)$	2209.6	$0.07^{+0.05}_{-0.05}$	$0.01^{+0.05}_{-0.01}$	<0.09	$0.03^{+0.05}_{-0.03}$	$0.05^{+0.05}_{-0.04}$	$0.03^{+0.03}_{-0.01}$
13114	$(\frac{51}{2}^+)$	1933.0	$0.19^{+0.05}_{-0.05}$	<0.04	$0.03^{+0.05}_{-0.03}$	$0.13_{-0.13}$ [b]	$0.05^{+0.49}_{-0.05}$	$0.04^{+0.05}_{-0.03}$
11181	$\frac{47}{2}^+$	1672.4 [b]	$0.22^{+0.05}_{-0.05}$	$0.09^{+0.17}_{-0.06}$		$0.12^{+0.16}_{-0.11}$	$0.08^{+0.23}_{-0.08}$	$0.10^{+0.10}_{-0.04}$
9509	$\frac{43}{2}^+$	1452.3	$0.35^{+0.05}_{-0.05}$	$0.21^{+0.20}_{-0.12}$	$0.12^{+0.13}_{-0.08}$	$0.07^{+0.05}_{-0.05}$	$0.12^{+0.12}_{-0.06}$	$0.09^{+0.04}_{-0.03}$
8056	$\frac{39}{2}^+$	442.3	$1.45^{+0.20}_{-0.20}$	$1.01^{+0.22}_{-0.16}$	$0.64^{+0.06}_{-0.06}$	$1.09^{+0.23}_{-0.18}$	$1.66^{+0.43}_{-0.28}$	$0.71^{+0.11}_{-0.11}$
6805	$\frac{35}{2}^+$	968.8	$2.38^{+0.10}_{-0.10}$	$0.72^{+0.24}_{-0.18}$	$0.62^{+0.13}_{-0.11}$	$0.61^{+0.10}_{-0.09}$	$0.64^{+0.16}_{-0.13}$	$0.63^{+0.09}_{-0.09}$
				$\pi=-,\ \alpha=+\frac{1}{2}$				
16184	$\frac{57}{2}^-$	2308.4 [a]	$0.17^{+0.39}_{-0.08}$					
13875	$\frac{53}{2}^-$	1861.2	$0.27^{+0.02}_{-0.02}$	$0.12^{+0.05}_{-0.04}$	$0.12^{+0.04}_{-0.04}$	$0.15^{+0.04}_{-0.04}$	$0.13^{+0.02}_{-0.03}$	$0.12^{+0.02}_{-0.02}$
12014	$\frac{49}{2}^-$	1780.8	$0.39^{+0.06}_{-0.06}$	$0.18^{+0.09}_{-0.06}$	$0.19^{+0.06}_{-0.05}$	$0.25^{+0.04}_{-0.04}$	$0.21^{+0.04}_{-0.04}$	$0.22^{+0.03}_{-0.03}$
		1557.6		$0.38^{+0.17}_{-0.14}$	$0.20^{+0.08}_{-0.07}$	$0.26^{+0.12}_{-0.07}$	$0.12^{+0.06}_{-0.06}$	
10456	$\frac{45}{2}^-$	1525.1	$0.50^{+0.05}_{-0.05}$	$0.07^{+0.08}_{-0.07}$	$0.09^{+0.05}_{-0.05}$	$0.21^{+0.07}_{-0.07}$	$0.19^{+0.07}_{-0.08}$	$0.13^{+0.03}_{-0.03}$
10233	$\frac{45}{2}^-$	1701.2	$0.66^{+0.05}_{-0.04}$	$0.50^{+0.06}_{-0.05}$	$0.54^{+0.06}_{-0.05}$	$0.40^{+0.13}_{-0.10}$	$0.37^{+0.11}_{-0.10}$	$0.49^{+0.07}_{-0.07}$
8931	$\frac{41}{2}^-$	1287.1	$0.61^{+0.07}_{-0.07}$	$0.27^{+0.07}_{-0.08}$	$0.11^{+0.06}_{-0.04}$	$0.34^{+0.07}_{-0.07}$	$0.24^{+0.12}_{-0.10}$	$0.22^{+0.04}_{-0.04}$
8532	$\frac{41}{2}^-$	1310.0	$1.29^{+0.25}_{-0.25}$	$0.51^{+0.13}_{-0.11}$	$0.44^{+0.10}_{-0.10}$	$0.90^{+0.22}_{-0.16}$	$0.39^{+0.13}_{-0.11}$	$0.48^{+0.07}_{-0.07}$
7644	$\frac{37}{2}^-$	1203.3	$1.25^{+0.21}_{-0.22}$		$0.38^{+0.17}_{-0.13}$			$0.38^{+0.17}_{-0.13}$
7222	$\frac{37}{2}^-$	480.2	$1.90^{+0.05}_{-0.05}$	$0.98^{+0.19}_{-0.14}$	$0.82^{+0.12}_{-0.11}$	$0.92^{+0.11}_{-0.09}$	$0.79^{+0.08}_{-0.07}$	$0.84^{+0.13}_{-0.13}$
6037	$\frac{33}{2}^-$	446.8	$3.13^{+0.03}_{-0.03}$		$0.27^{+0.06}_{-0.04}$	$0.44^{+0.07}_{-0.07}$		$0.34^{+0.05}_{-0.05}$
				$\pi=-,\ \alpha=-\frac{1}{2}$				
11576	$\frac{47}{2}^-$	1736.8 [a]	$0.28^{+0.05}_{-0.04}$					
9840	$(\frac{43}{2}^-)$	1590.1	$0.56^{+0.11}_{-0.11}$	$0.60^{+0.25}_{-0.17}$	$0.52^{+0.14}_{-0.11}$	$0.27^{+0.13}_{-0.17}$	$0.37^{+0.11}_{-0.08}$	$0.40^{+0.07}_{-0.06}$
8362	$\frac{39}{2}^-$	1391.6 [a]	$0.52^{+0.10}_{-0.08}$					
8250	$\frac{39}{2}^-$	1508.2	$0.99^{+0.05}_{-0.05}$	$0.78^{+0.13}_{-0.12}$	$0.64^{+0.10}_{-0.09}$	$0.60^{+0.13}_{-0.11}$	$0.69^{+0.13}_{-0.11}$	$0.67^{+0.10}_{-0.10}$
6971	$\frac{35}{2}^-$	1196.8	$1.03^{+0.27}_{-0.27}$	$0.39^{+0.39}_{-0.22}$	$0.71^{+0.89}_{-0.31}$	$0.44^{+0.39}_{-0.20}$	$0.47^{+0.49}_{-0.22}$	$0.45^{+0.23}_{-0.11}$
6742	$\frac{35}{2}^-$	705.0	$2.37^{+0.06}_{-0.06}$	$0.55^{+0.16}_{-0.12}$	$0.51^{+0.05}_{-0.05}$	$0.44^{+0.04}_{-0.04}$	$0.50^{+0.06}_{-0.06}$	$0.48^{+0.07}_{-0.07}$
5774	$\frac{31}{2}^-$	475.0	$1.76^{+0.15}_{-0.15}$			$0.42^{+0.27}_{-0.18}$	$0.39^{+0.15}_{-0.16}$	$0.40^{+0.13}_{-0.12}$

[a]Due to a lack of feeding information about this state, only an effective lifetime could be determined.
[b]Lifetime determined using gates on transitions above the line being investigated.

figures are listed in Table V along with the maximum spin possible within the configuration and the shorthand label. These labels $[p,n]^\alpha$ indicate the number of protons (p) and neutrons (n) in the unique-parity $g_{9/2}$ orbitals and the sign of the total signature α of the configuration. The Q_t values calculated for these configurations using Eqs. (67) and (68) of Ref. [26] are shown as curves in the bottom panels of Figs. 7–10.

B. Positive-parity structures

The energy minus rigid rotor graphs for the $\pi=+,\ \alpha=+\frac{1}{2}$ states shown in the middle panel of Fig. 7 illustrate the rather complex band structure in ^{87}Nb. The relatively frequent slope changes generally indicate band crossings and show that no single configuration remains yrast for long. The lowest positive-parity structure (assigned $\pi g_{9/2}$ in Ref. [4]

TABLE III. The electric quadrupole transition strengths and transition quadrupole moments deduced from the lifetime measurements. A value of 5/2 was used for K in order to determine the transition quadrupole moments. (1 W.u.$=22.9\ e^2\ \mathrm{fm}^4$)

E_x (keV)	I_i^π	E_γ (keV)	τ (ps)	$B(E2)$(W.u.)	$Q_t(e\ \mathrm{b})$
		$\pi=+,\ \alpha=+\frac{1}{2}$			
11945	$\frac{49}{2}^+$	1954.3 [a]	$0.04^{+0.05}_{-0.03}$	>17.9	>1.08
9991	$\frac{45}{2}^+$	1565.1	$0.32^{+0.05}_{-0.05}$	$11.8^{+2.0}_{-1.5}$	$0.88^{+0.07}_{-0.06}$
8426	$\frac{41}{2}^+$	1291.5	$0.58^{+0.09}_{-0.09}$	$10.4^{+1.8}_{-1.4}$	$0.83^{+0.07}_{-0.06}$
7134	$\frac{37}{2}^+$	1298.1	$0.43^{+0.06}_{-0.06}$	$16.4^{+2.9}_{-2.1}$	$1.05^{+0.09}_{-0.07}$
5836	$\frac{33}{2}^+$	1248.1 [b]	$0.42^{+0.13}_{-0.08}$	$26.9^{+6.3}_{-6.3}$	$1.36^{+0.15}_{-0.17}$
8566	$(\frac{41}{2}^+)$	1431.8	$0.92^{+0.20}_{-0.14}$	$6.4^{+1.1}_{-1.1}$	$0.65^{+0.06}_{-0.06}$
7614	$\frac{37}{2}^+$	1777.7	$0.48^{+0.10}_{-0.07}$	$1.9^{+0.3}_{-0.3}$	$0.36^{+0.03}_{-0.03}$
		$\pi=+,\ \alpha=-\frac{1}{2}$			
17922	$(\frac{59}{2}^+)$	2598.4 [a]	$0.04^{+0.09}_{-0.04}$	$3.8^{+3.8}_{-2.0}$	>0.34
15324	$(\frac{55}{2}^+)$	2209.6	$0.03^{+0.03}_{-0.01}$	$22.5^{+11.3}_{-11.3}$	$1.21^{+0.27}_{-0.35}$
13114	$(\frac{51}{2}^+)$	1933.0	$0.04^{+0.05}_{-0.03}$	$33.0^{+99.1}_{-18.3}$	$1.47^{+1.47}_{-0.49}$
11181	$\frac{47}{2}^+$	1672.4 [b]	$0.10^{+0.10}_{-0.04}$	$27.2^{+18.2}_{-13.6}$	$1.34^{+0.39}_{-0.39}$
9509	$\frac{43}{2}^+$	1452.3	$0.09^{+0.04}_{-0.03}$	$39.9^{+19.9}_{-12.2}$	$1.62^{+0.37}_{-0.27}$
8056	$\frac{39}{2}^+$	1251.2	$0.71^{+0.11}_{-0.11}$	$11.3^{+2.0}_{-1.4}$	$0.87^{+0.07}_{-0.06}$
6805	$\frac{35}{2}^+$	1188.6	$0.63^{+0.09}_{-0.09}$	$5.0^{+0.9}_{-0.6}$	$0.58^{+0.05}_{-0.04}$
		$\pi=-,\ \alpha=+\frac{1}{2}$			
16184	$\frac{57}{2}^-$	2308.4 [a]	$0.17^{+0.39}_{-0.08}$	$3.2^{+2.8}_{-2.2}$	>0.25
13875	$\frac{53}{2}^-$	1861.2	$0.12^{+0.02}_{-0.02}$	$13.3^{+2.6}_{-1.9}$	$0.93^{+0.09}_{-0.07}$
12014	$\frac{49}{2}^-$	1780.8	$0.22^{+0.03}_{-0.03}$	$5.1^{+0.8}_{-0.6}$	$0.58^{+0.04}_{-0.04}$
		1557.6		$7.8^{+1.2}_{-0.9}$	$0.71^{+0.05}_{-0.04}$
10456	$\frac{45}{2}^-$	1525.1	$0.13^{+0.03}_{-0.03}$	$13.6^{+4.1}_{-2.3}$	$0.95^{+0.13}_{-0.09}$
10233	$\frac{45}{2}^-$	1701.2	$0.49^{+0.07}_{-0.07}$	$3.2^{+0.5}_{-0.4}$	$0.46^{+0.04}_{-0.03}$
8931	$\frac{41}{2}^-$	1287.1	$0.22^{+0.04}_{-0.04}$	$24.4^{+3.8}_{-3.7}$	$1.27^{+0.10}_{-0.10}$
8532	$\frac{41}{2}^-$	1310.0	$0.48^{+0.07}_{-0.07}$	$11.0^{+1.8}_{-1.4}$	$0.85^{+0.07}_{-0.06}$
7644	$\frac{37}{2}^-$	1253.7	$0.38^{+0.17}_{-0.13}$	$3.5^{+1.8}_{-1.0}$	$0.49^{+0.11}_{-0.08}$
		1203.3		$7.3^{+3.8}_{-2.2}$	$0.70^{+0.16}_{-0.12}$
7222	$\frac{37}{2}^-$	1185.2	$0.84^{+0.13}_{-0.13}$	$3.1^{+0.5}_{-0.4}$	$0.46^{+0.04}_{-0.03}$
6037	$\frac{33}{2}^-$	1028.8	$0.34^{+0.05}_{-0.05}$	$8.4^{+1.4}_{-1.0}$	$0.76^{+0.06}_{-0.05}$
		$\pi=-,\ \alpha=-\frac{1}{2}$			
11576	$\frac{47}{2}^-$	1736.8 [a]	$0.28^{+0.05}_{-0.04}$	$8.0^{+1.3}_{-1.2}$	>0.67
9840	$(\frac{43}{2}^-)$	1590.1	$0.40^{+0.07}_{-0.06}$	$5.4^{+1.0}_{-0.08}$	$0.60^{+0.05}_{-0.05}$
8362	$\frac{39}{2}^-$	1391.6 [a]	$0.52^{+0.10}_{-0.08}$	$8.2^{+1.5}_{-1.3}$	>0.68
8250	$\frac{39}{2}^-$	1508.2	$0.67^{+0.10}_{-0.10}$	$6.3^{+1.1}_{-0.8}$	$0.65^{+0.05}_{-0.04}$
6971	$\frac{35}{2}^-$	1196.8	$0.45^{+0.23}_{-0.11}$	$19.3^{+6.2}_{-6.6}$	$1.15^{+0.17}_{-0.21}$
6742	$\frac{35}{2}^-$	1151.8	$0.48^{+0.07}_{-0.07}$	$10.0^{+1.7}_{-1.3}$	$0.83^{+0.07}_{-0.06}$
5774	$\frac{31}{2}^-$	997.1	$0.40^{+0.13}_{-0.12}$	$50.7^{+21.7}_{-12.4}$	$1.88^{+0.37}_{-0.25}$

[a]Due to a lack of feeding information about this state, only an effective lifetime could be determined.
[b]Lifetime determined using gates on gansitions above the line being investigated.

and labeled 13 in Fig. 2) is built on the $\frac{9}{2}^+$ isomer that lies only 3 keV above the $\frac{1}{2}^-$ ground state. Its energy graph rises rapidly indicating a moment of inertia significantly smaller than that of the reference. The slope drops at the $\frac{21}{2}^+$ state and then returns to nearly its original value at the $\frac{25}{2}^+$ state, suggesting a change in structure.

The yrast line bends sharply away from band 13 at the $\frac{17}{2}^+$ state, to a structure (band 11) with a significantly larger moment of inertia, close to that of the reference. This has been attributed to a $g_{9/2}$ neutron alignment at the $\frac{21}{2}^+$ state (band 11) based on the relatively small g factor of $+0.41(13)$ and shell-model calculations in the $(g_{9/2},p_{1/2})$ model space [8]. It is consistent with the expectation that the lowest proton $g_{9/2}$ alignment would be Pauli-blocked. The CNS approach is not applicable to these states because of the importance of pairing at lower spins.

The shape of the calculated energy curve for the $[3,8]^+$ configuration is similar to that of band 11 up to about the $\frac{33}{2}^+$

TABLE IV. $B(M1)$ strengths inferred from the measured lifetimes assuming mixing ratios δ of zero, grouped by the bands between which the decays occur.

E_x (keV)	I_i^π	E_γ (keV)	$B(M1)$ (μ_N^2)
		$1 \Leftrightarrow 3$	
8931	$\frac{41}{2}^-$	568.9	$0.425^{+0.094}_{-0.065}$
8362	$\frac{39}{2}^-$	718.2	$0.110^{+0.020}_{-0.018}$
7644	$\frac{37}{2}^-$	673.4	$0.099^{+0.051}_{-0.030}$
6971	$\frac{35}{2}^-$	529.9	$0.341^{+0.110}_{-0.115}$
5774	$\frac{31}{2}^-$	475.0	$0.745^{+0.319}_{-0.183}$
		$1 \Leftrightarrow 5$	
3218	$\frac{21}{2}^-$ [a]	313.6	$0.200^{+0.040}_{-0.029}$
		$3 \Leftrightarrow 4$	
10456	$\frac{45}{2}^-$	616.3	$1.108^{+0.332}_{-0.208}$
9840	$(\frac{43}{2}^-)$	908.8	$0.072^{+0.013}_{-0.011}$
7644	$\frac{37}{2}^-$	902.4	$0.074^{+0.038}_{-0.023}$
		$2 \Leftrightarrow 6$	
2411	$\frac{17}{2}^-$ [a]	136.0	$0.108^{-0.010}_{-0.008}$
2275	$\frac{15}{2}^-$ [a]	299.4	$0.040^{+0.006}_{-0.004}$
1602	$\frac{11}{2}^-$ [a]	434.6	$0.006^{+0.003}_{-0.001}$
838	$\frac{7}{2}^-$ [a]	505.4	$0.007^{+0.003}_{-0.002}$
		$3 \Leftrightarrow 5$	
8931	$\frac{41}{2}^-$	399.3	$0.694^{+0.154}_{-0.107}$
		$4 \Leftrightarrow 5$	
9840	$(\frac{43}{2}^-)$	1308.1	$0.024^{+0.004}_{-0.004}$
8532	$\frac{41}{2}^-$	282.0	$2.279^{+0.389}_{-0.290}$
8250	$\frac{39}{2}^-$	1028.0	$0.006^{+0.001}_{-0.001}$
7222	$\frac{37}{2}^-$	480.2	$0.510^{+0.093}_{-0.068}$
6742	$\frac{35}{2}^-$	705.0	$0.200^{+0.034}_{-0.025}$
6037	$\frac{33}{2}^-$	446.8	$1.710^{+0.295}_{-0.219}$
5590	$\frac{31}{2}^-$	582.0	$0.322^{+0.092}_{-0.058}$
		Misc. $\pi=-$	
6742	$\frac{35}{2}^-$	351.3	$0.357^{+0.061}_{-0.045}$
3218	$\frac{21}{2}^-$ [a]	637.9	$0.003^{+0.001}_{-0.001}$
3218	$\frac{21}{2}^-$ [a]	231.5	$0.174^{+0.035}_{-0.025}$
		$8 \Leftrightarrow 12$	
8426	$\frac{41}{2}^+$	369.6	$0.757^{+0.139}_{-0.102}$
		$11 \Leftrightarrow 12$	
7134	$\frac{37}{2}^+$	329.3	$1.006^{+0.163}_{-0.123}$
6805	$\frac{35}{2}^+$	968.8	$0.056^{+0.009}_{-0.007}$
5836	$\frac{33}{2}^+$	219.8	$0.510^{+0.120}_{-0.121}$
4588	$\frac{29}{2}^+$ [a]	291.1	$0.515^{+0.257}_{-0.129}$
3443	$\frac{25}{2}^+$ [a]	226.5	$1.174^{+0.107}_{-0.090}$
3217	$\frac{23}{2}^+$ [a]	728.3	$0.174^{+0.058}_{-0.035}$
		$12 \Leftrightarrow 13$	
3217	$\frac{23}{2}^+$ [a]	358.1	$0.093^{+0.031}_{-0.019}$
2858	$\frac{21}{2}^+$ [a]	370.2	$0.620^{+0.867}_{-0.228}$
		Misc. $\pi=+$	
9509	$\frac{43}{2}^+$	641.1	$0.193^{+0.096}_{-0.059}$
		499.6	$1.319^{+0.659}_{-0.406}$
7614	$\frac{37}{2}^+$	808.9	$0.123^{+0.021}_{-0.021}$

[a] $B(M1)$ strength determined using lifetimes from prior work [4].

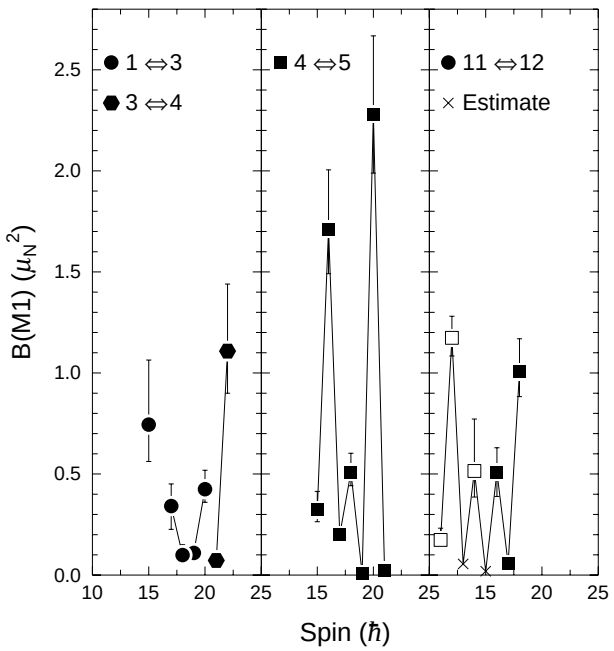

FIG. 6. $B(M1)$ transition strengths between the indicated bands plotted at the spin value intermediate between those of the initial and final levels. Filled (open) symbols represent values based on lifetimes measured in this work (measured previously). The estimated values are discussed in the text.

state. The change in slope of the experimental curve above this suggests a configuration change. The $[3,6]^+$ configurations, which are predicted to become yrast at about the $\frac{29}{2}^+$ state, are candidates for the high-spin portion of band 11. The exact crossing point is sensitive to the single-particle energies used in the model. The two variants of the $[3,6]^+$ configurations stem from a second minima in the potential energy surface in the CNS approach and may be interpreted as one configuration $[3,6]_a^+$ terminating at $I=\frac{53}{2}^+$ with the two proton holes coupling to $I=4$, and another $[3,6]_b^+$ terminating at $I=\frac{45}{2}^+$ with the two proton holes coupling to $I=0$. The existence of two variants of the $[3,6]^+$ configuration with similar energies may account for band 8, as well. If so, the observed termination at the $\frac{53}{2}^+$ state is somewhat more unfavored than predicted. Both the $[4,7]^+$ and $[5,6]^+$ configurations (or some mixture of them) are candidates for band 7. Both theoretical bands terminate at $\frac{61}{2}^+$, the last spin observed in band 7.

Although the moment of inertia is small, the transition quadrupole moments Q_t between the lowest states in band 13, shown in the bottom panel of Fig. 7, are the strongest ones which have been observed in ^{87}Nb. Band 11 has a significantly higher and relatively constant moment of inertia, but curiously its Q_t values are lower. There is no overlap between the present and previous lifetime measurements, but the inferred Q_t values appear to join smoothly. A change of slope does occur in the Q_t graph for band 11 about where the energy graph changes slope, indicating a band crossing. The last three Q_t values drop significantly and follow relatively well the predictions for the $[3,6]_b^+$ configuration. This supports the suggestion from the energy graph that band 11 rep-

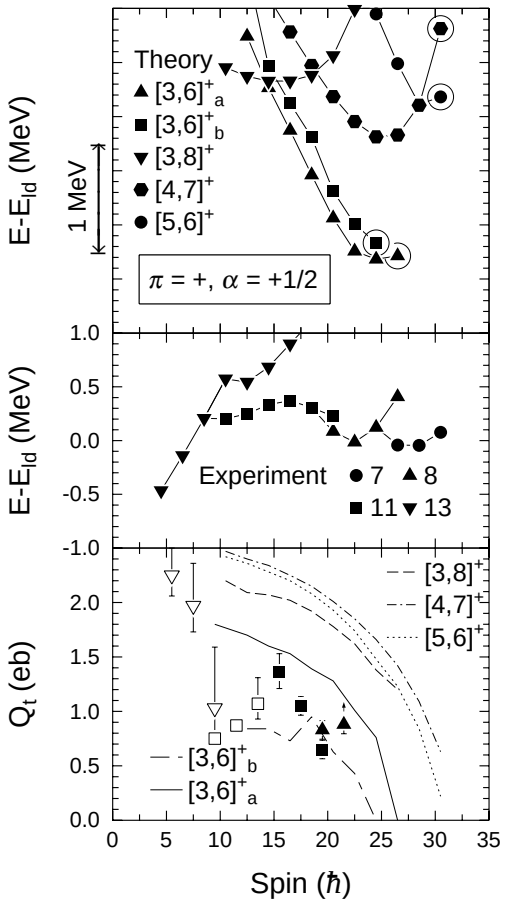

FIG. 7. In the top panel, the results of CNS approach calculations for $\pi=+$, $\alpha=+\frac{1}{2}$ configurations are plotted against spin with the energy of a ''standard'' rigid rotor subtracted to remove the dominant quadratic dependence on spin. The same energy window is shown in Figs. 8–10. In the middle panel, the observed states with the same combination of parity and signature are plotted in the same manner. Q_t values for the transitions between these states are plotted against the spin value intermediate between those of the initial and final levels in the bottom panel along with CNS approach predictions. Filled (open) symbols represent values based on present (previous) work.

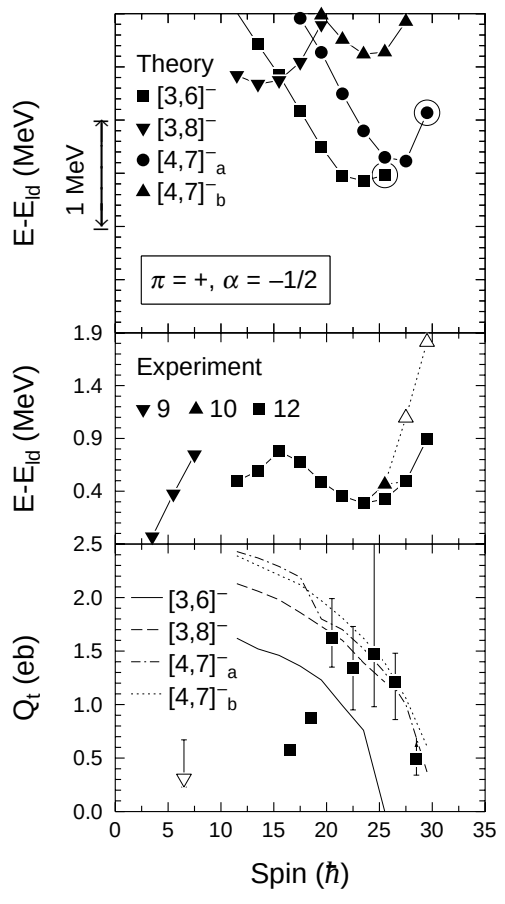

FIG. 8. Same as Fig. 7, but for the $\pi=+$, $\alpha=-\frac{1}{2}$ states.

resents the terminating portion of the $[3,6]_b^+$ structure. The Q_t values in band 8 lie somewhat below those predicted for the $[3,6]_a^+$ configuration and could not be measured high enough in spin to test the predicted falloff towards termination.

Among the signature $\alpha=-\frac{1}{2}$ levels, the graph of band 9 in Fig. 8 exactly parallels that of the lower portion of band 13 in Fig. 7 with an offset (signature splitting) of about 700 keV. This is quite consistent with the systematics of large signature splitting in $\pi g_{9/2}$ bands in this region [15]. This relation and the existence of $\Delta I=1$ decays connecting bands 9 and 13, thus suggesting that they are signature partners. Band 9 could not be observed to higher spins, probably because the large signature splitting makes it energetically unfavored. In fact, no $\frac{19}{2}^+$ state is known in ^{87}Nb.

A number of $\Delta I=1$ transitions connect bands 11 and 12 up to the $\frac{37}{2}^+$ level and their energy graphs are relatively similar. Thus, band 12 is likely the signature partner of band 11 over this range, with significantly less signature splitting of about 300 keV. An alternating pattern can be seen in the $M1$ strengths between bands 11 and 12 (see Fig. 6), although two of the lifetimes are not known. The missing $B(M1)$ values can be estimated by assuming that the in-band $E2$ decays have Q_t values similar to those of their neighbors ($\sim$0.5 e b). These estimates are shown with ''$\times$'' symbols in Fig. 6. Even though the estimate may be uncertain by as much as a factor of 2, it does confirm the alternating $B(M1)$ pattern. The strong $B(M1)$ values, which reach almost single-particle strength, occur among the low-energy transitions from band 11 to 12, while the higher-energy transitions from band 12 to 11 have the much weaker $B(M1)$ values. Such alternations have been seen in a number of bands in $A\sim80$ nuclei, including the neighbors ^{86}Nb [2] and ^{86}Zr [32]. They are generally correlated with signature splitting and can be understood in both the particle-rotor model [33] and the Interacting Boson Fermion Model [32].

The shape of the $[3,8]^-$ energy curve is similar to the lower-spin portion of band 12. As in the $\alpha=+1/2$ case, the crossing with the $[3,6]^-$ configuration may explain the change in slope of band 12 at the $\frac{31}{2}^+$ state. At the highest spins, the $[4,7]_a^-$ configuration becomes yrast and terminates at the $\frac{59}{2}^+$ level, the highest $\alpha=-1/2$ level observed experimentally.

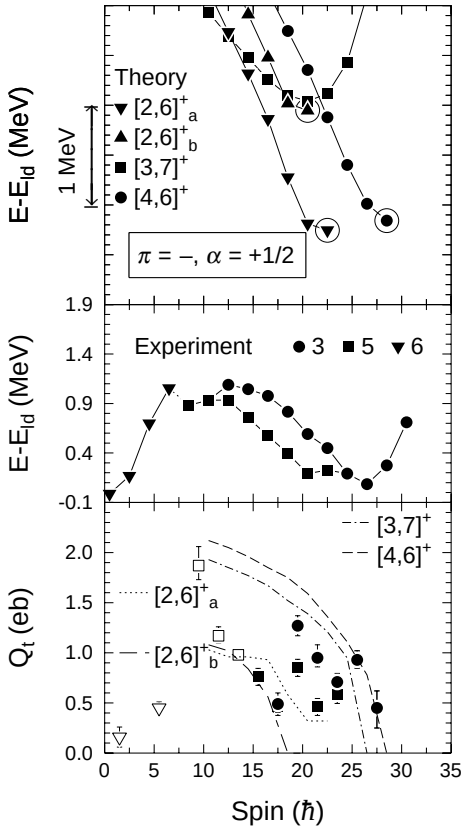

FIG. 9. Same as Fig. 7, but for the $\pi=-$, $\alpha=+\frac{1}{2}$ states.

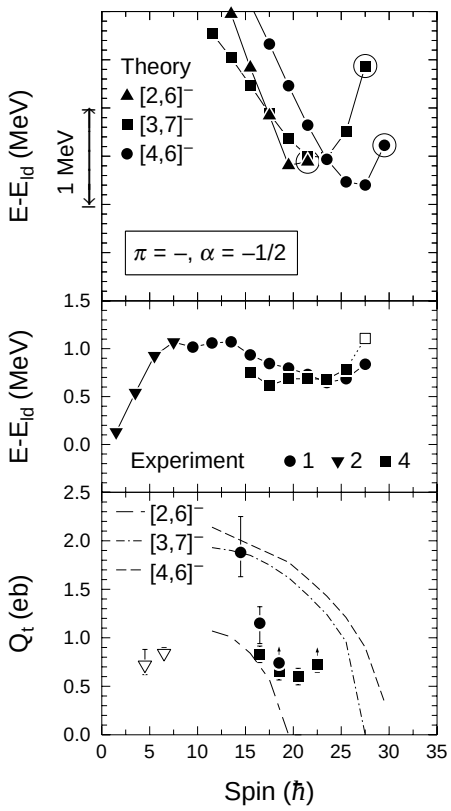

FIG. 10. Same as Fig. 7, but for the $\pi=-$, $\alpha=-\frac{1}{2}$ states.

Most of the measured Q_t values follow those predicted for the $[4,7]^-$ configurations very well, including the fall towards termination. This could be explained if the $[4,7]^-$ configurations were somewhat lower relative to the $[3,6]^-$ one due to small variations in the single-particle energies. In any event, the falling experimental Q_t values definitely support a band termination interpretation.

In summary, the band structure of the positive-parity states in ^{87}Nb becomes more complex above the $\frac{17}{2}^+$ level. The CNS approach calculations provide a reasonable interpretation in terms of a number of competing configurations which become yrast in different spin ranges. Signature-partner theoretical structures can generally account for the signature-partner experimental bands. Small adjustments in the model parameters would probably lead to better agreement by changing somewhat the relative energies of the configurations. The measured transition quadrupole moments Q_t in bands 11 and 12 fall significantly towards the highest spins in agreement with theoretical predictions and strongly support a band termination interpretation.

C. Negative-parity structures

The relative energy graphs for the lowest negative-parity bands (2 and 6) (middle panels in Figs. 9 and 10) rise rapidly with spin with about the same slope (and hence moment of inertia) as the lowest positive-parity bands. They also appear to be signature partners, but with essentially no signature splitting, resulting from small splitting of the low-j $N=3$ orbitals. This is in contrast to the positive-parity case where the large splitting between bands 9 and 13 reflects the large splitting of the $g_{9/2}$ signature-partner orbitals and possibly deformation effects (as follows from the Q_t values for these bands). This, too, is consistent with the $A\sim 80$ systematics. The transition quadrupole moments Q_t are much smaller than the corresponding ones in band 13 and mostly larger than the one measured Q_t value in band 9, possibly indicating that vibrations can play an important role in their structure. It has been proposed that the lowest $\frac{1}{2}^-$ and $\frac{5}{2}^-$ states are based on different Nilsson configurations ($[301]\frac{1}{2}^-$ and $[303]\frac{5}{2}^-$) because of the low collectivity of the 333 keV transition between them, which is nearly two orders of magnitude lower than that predicted in $(g_{9/2},p_{1/2})$ shell-model calculations [6]. The kink in the energy curve for band 6 at this point may be consistent with a configuration change or, alternatively, with vibrational effects. Perhaps this is another indication that a wider basis shell-model calculation is needed at $N=46$. Also, the rising Q_t trend in band 6 contrasts sharply with the falling pattern of Q_t in band 13.

Clearly a change occurs in the band structure and moments of inertia at about 2.4 MeV, where three quasiparticle (qp) structures become energetically favored. The 2411 keV $\frac{17}{2}^-$ state has been assigned a dominant $\pi(g_{9/2})_{9/2}\otimes\nu(g_{9/2}p_{1/2})_4$ structure on the basis of similarities of its weak, opportunistic decay pattern with shell-model predictions. The limited $(g_{9/2},\ p_{1/2})$ model space may explain the difference between the predicted g factor of $+0.44$ and the measured [8] value of $+0.82(10)$. The g factor of the $\frac{29}{2}^-$ state in this band has been measured to be $+0.56(16)$ [10].

TABLE V. Calculated configurations in ^{87}Nb. Configuration labels are given in the first column. The detailed structure of the terminating states of these configurations (relative to a spherical ^{80}Zr core) is given in the second column and the calculated maximum spins I^{π}_{max} are given in the last column.

	Configuration	I^{π}_{max} ($\hbar$)
	$(\pi=+,\alpha=+1/2)$	
$[3,6]^+_a$	$\pi(g_{9/2})^3_{10.5}(f_{5/2})^{-2}_4 \otimes \nu(g_{9/2})^6_{12}$	26.5
$[3,6]^+_b$	$\pi(g_{9/2})^3_{10.5}(f_{5/2})^{-2}_0 \otimes \nu(g_{9/2})^6_{12}$ [a]	22.5
$[3,8]^+$	$\pi(g_{9/2})^3_{10.5}(f_{5/2})^{-2}_4 \otimes \nu(g_{9/2})^8_8(f_{5/2})^{-2}_4$	26.5
$[4,7]^+$	$\pi(g_{9/2})^4_{12}(f_{5/2})^{-2}_4(p_{3/2})^{-1}_{1.5} \otimes \nu(g_{9/2})^7_{10.5}(f_{5/2})^{-1}_{2.5}$	30.5
$[5,6]^+$	$\pi(g_{9/2})^5_{12.5}(f_{5/2})^{-2}_4(p_{3/2})^{-2}_2 \otimes \nu(g_{9/2})^6_{12}$	30.5
	$(\pi=+,\alpha=-1/2)$	
$[3,6]^-$	$\pi(g_{9/2})^3_{9.5}(f_{5/2})^{-2}_4 \otimes \nu(g_{9/2})^6_{12}$	25.5
$[3,8]^-$	$\pi(g_{9/2})^3_{9.5}(f_{5/2})^{-2}_4 \otimes \nu(g_{9/2})^8_8(f_{5/2})^{-2}_4$	25.5
$[4,7]^-_a$	$\pi(g_{9/2})^4_{12}(f_{5/2})^{-2}_4(p_{1/2})^{-1}_{0.5} \otimes \nu(g_{9/2})^7_{10.5}(f_{5/2})^{-1}_{2.5}$	29.5
$[4,7]^-_b$	$\pi(g_{9/2})^4_{11}(f_{5/2})^{-2}_4(p_{3/2})^{-1}_{1.5} \otimes \nu(g_{9/2})^7_{10.5}(f_{5/2})^{-1}_{2.5}$	29.5
	$(\pi=-,\alpha=+1/2)$	
$[2,6]^+_a$	$\pi(g_{9/2})^2_8(f_{5/2})^{-1}_{2.5} \otimes \nu(g_{9/2})^6_{12}$	22.5
$[2,6]^+_b$	$\pi(g_{9/2})^2_8(p_{3/2})^{-1}_{1.5} \otimes \nu(g_{9/2})^6_{11}$	20.5
$[3,7]^+$	$\pi(g_{9/2})^3_{9.5}(f_{5/2})^{-2}_4 \otimes \nu(g_{9/2})^7_{10.5}(f_{5/2})^{-1}_{2.5}$	26.5
$[4,6]^+$	$\pi(g_{9/2})^4_{12}(f_{5/2})^{-2}_4(p_{3/2})^{-1}_{0.5} \otimes \nu(g_{9/2})^6_{12}$	28.5
	$(\pi=-,\alpha=-1/2)$	
$[2,6]^-$	$\pi(g_{9/2})^2_8(f_{5/2})^{-1}_{2.5} \otimes \nu(g_{9/2})^6_{11}$	21.5
$[3,7]^-$	$\pi(g_{9/2})^3_{10.5}(f_{5/2})^{-2}_4 \otimes \nu(g_{9/2})^7_{10.5}(f_{5/2})^{-1}_{2.5}$	27.5
$[4,6]^-$	$\pi(g_{9/2})^4_{12}(f_{5/2})^{-2}_4(p_{3/2})^{-1}_{1.5} \otimes \nu(g_{9/2})^6_{12}$	29.5

[a] $[3,6]^+_b$ is the second minima in the energy surface of $[3,6]^+_a$.

Above the one qp region, two bands of each signature occur at relatively similar energies and cross around $\frac{47}{2}$. Bands 1 and 3 and bands 4 and 5 are connected by a number of $\Delta I=1$ transitions suggesting that these pairs form signature partners. An alternating pattern is seen in the $B(M1)$ strengths of the transitions connecting bands 4 and 5, as would be expected for the pair exhibiting the larger signature splitting. Several of the $B(M1)$ values are comparable with, or exceed, the single-particle estimate. The weaker ''strong'' $B(M1)$ value occurs at the change in slope of the energy graph for band 4. Above this, the energy curves of both bands 3 and 5 fall faster than those of bands 1 and 4.

In theoretical calculations for the $\pi=-$ and $\alpha=+1/2$ states, a less collective yrast configuration, $[2,6]^+_a$ is predicted. The lack of a corresponding observed band could be explained by the difficulty of populating such a weakly collective structure in a fusion-evaporation reaction. Other, more collective, configurations are better candidates for identification with the experimentally observed bands. The best choice for most of the band 5 appears to be the $[3,7]^+$ configuration, since it is closer in structure to what was previously proposed for the $\frac{17}{2}^-$ state. Experimentally, band 5 merges with band 3 at the $\frac{49}{2}^-$ state and has not been observed to termination. In addition, the analysis of kinematic and dynamic moments of inertia in band 5 indicates that at $I>20$, either its structure changes or an interaction with another configuration or aligned state takes place, as seen in Fig. 11. The $[4,6]^+$ configuration may be the best match for band 3, although it is possible that the low-spin part of this band is built on another configuration, maybe $[5,7]^+$ or a second $[3,7]^+$, although these are energetically too high with the present parameters and not considered in the present approach. This is because the structure change is seen in this band via $J^{(2)}$ and $J^{(1)}$ at $I\approx 22$ in Fig. 11. In any case, the observed $\frac{61}{2}^-$ state must belong to another structure, since the $[4,6]^+$ configuration terminates at the $\frac{57}{2}^-$ state. The two highest Q_t values in band 3 fall towards termination and agree well with the predictions for the $[4,6]^+$ configuration. The Q_t values for band 5 lie between the predictions for the $[2,6]^+$, $[3,7]^+$, and $[4,6]^+$ configurations. Their behavior (which is consistent with that of $J^{(2)}$ and $J^{(1)}$) suggests several structural changes with spin.

The $[2,6]^-$, $[3,7]^-$, and $[4,6]^-$ configurations are graphed in Fig. 10 for comparison with experiment. These are the signature partners of the ones discussed above, and their signature splitting is defined both by splittings of the low-j $N=3$ orbitals and deformation differences. The $[3,7]^-$ configuration, which is a signature partner of the $[3,7]^+$ one, is a candidate to represent band 4, which is the signature partner of band 5. The $[3,7]^-$ energy graph rises toward termination at the $\frac{55}{2}^-$ level, and band 5 also rises towards the last, tentative, state at $\frac{55}{2}^-$, although not as steeply. Likewise, the $[4,6]^-$ configuration may represent band 1 like its signature partner $[4,6]^+$ and band 3. Although the energy curve for band 1 starts rising towards the highest observed spin in $\frac{55}{2}^-$, no counterpart has been observed for the termi-

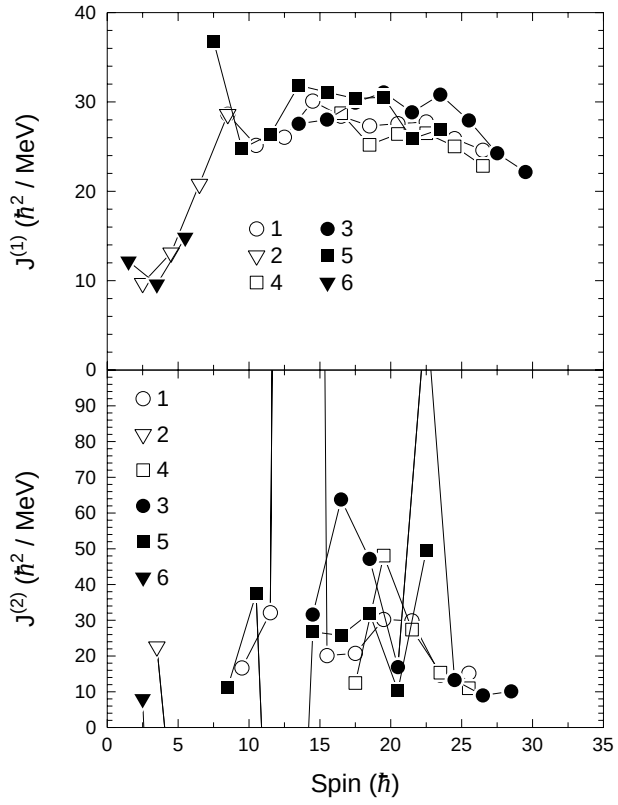

FIG. 11. The kinematic $J^{(1)}$ and dynamic $J^{(2)}$ moments of inertia plotted against spin. Some points are off the range.

nating state at $\frac{59}{2}^-$ as seen in the calculations.

The experimental Q_t values generally lie within the range predicted for the three theoretical configurations, but it was not possible to measure them close to the predicted terminations. At lower spins, the Q_t values in band 1 drop as if approaching a termination at $\frac{39}{2}^-$. This may indicate some change in microscopic structure, although there is only a slight irregularity in the energy graph.

Overall, there is a reasonable agreement between the CNS approach calculations and experiment for the negative-parity states. The measured transition quadrupole moments are within the range predicted theoretically, but the detailed agreement is not as good as for the positive-parity bands. Several of the energy graphs suggest band terminations, and one of these is confirmed by the Q_t values. The variations of the Q_t values hint at a number of microscopic structure changes, which in many (but not all) cases correlate with changes seen in the dynamic and kinematic moments of inertia. This might explain why the experimental Q_t values (extracted from $B(E2)$ values) are a factor of 2 smaller than predicted ones in a number of cases. This is because the matrix element $B(E2)$ of the $E2(I \rightarrow I-2)$ transition depends on the wave functions of the I and $I-2$ states, which in the band crossing region may differ considerably. On the other hand, the calculation of the Q_t values in the CNS approach within the rigid rotor limit is based on the assumption that the difference in the wave functions of the I and $I-2$ states is small. Thus, it is not surprising that the calculations overestimate the experimental Q_t values in the regions of structure change.

V. SUMMARY

The high-spin structure of ^{87}Nb was investigated in two experiments using GAMMASPHERE and the MICROBALL after production in the ^{58}Ni(^{32}S,3p) reaction at 135 MeV. The first experiment, using a thin, self-supporting ^{58}Ni target, led to a considerable expansion and refinement of the energy level scheme and to the firm assignment of many spins from the DCO ratios. A backed target was used in the second experiment to measure the mean lifetimes of many states in the sub-picosecond range with the DSAM. Particle-gated triple γ coincidences gave clean line shapes in most cases. Line shapes were fitted independently at four angles of observation, then compared and averaged. Approximate Doppler-shift correction for the high-energy lines made it possible to gate above a number of transitions and obtain line shapes that are independent of the uncertainties of side feeding. A comparison of these fits with line shapes gated from below led to an estimate of side-feeding lifetimes in this reaction for use with the line shapes that could not be gated from above.

The results of this work confirm that the transitional nature of $N=46$ ^{87}Nb extends up to the highest spins observed. Sequences of states are observed which increase in energy as rotational bands with moments of inertia both smaller and larger than the typical reference value of $\hbar^2/2J_{\rm rig}$ $=18.9$ keV. However, abrupt changes in the moments of inertia, indicating structural changes, occur repeatedly in the decay sequences. The lifetimes imply a rather modest average deformation of $\beta_2 \sim 0.1$, but with considerable variation from state to state, reflecting those changes in many cases. Strong alternations were observed in the $B(M1)$ strengths of transitions between some pairs of bands.

Calculations were performed within the cranked Nilsson-Strutinsky approach to provide a framework for understanding the rather complex behavior of both the energies and lifetimes. A general characteristic of these calculations is that the energies, relative to a rigid rotor, fall with increasing spin and then level off and rise approaching the fully aligned, or terminating, state. The pattern slides to higher spins for configurations with more particles promoted from f-p orbitals to the unique-parity $g_{9/2}$ orbital. There is evidence for this pattern in the irregularities observed in all the yrast lines, although it is clearest in the $\pi=+$, $\alpha=-\frac{1}{2}$ and $\pi=-$, $\alpha=+\frac{1}{2}$ states. In a number of cases, the bands have been observed up to the terminating states.

Further evidence for band terminations comes from the transition quadrupole moments Q_t inferred from the lifetimes measured in the present work. At high spin, with a few exceptions, measured Q_t values fall with increasing spin, reflecting an approach to band termination. Configurations with larger numbers of particles excited from the $N=3$ shell to the $g_{9/2}$ subshell start from higher values of Q_t (more deformed) and fall to zero at higher spins. The measured Q_t

values in bands 3, 11, and 12 do fall rapidly with increasing spin, in strong support of the band termination interpretation.

The picture is not perfect, however. Some of the complications in comparing theory with experiment arise from the relatively large number of possible configurations in this odd *A* nucleus. Small changes in the model parameters (for example, Nilsson potential parameters) can change the qualitative appearance of the calculated yrast line. In spite of these difficulties, the comparison of the measured level scheme and lifetimes with the CNS approach calculations does illustrate rather clearly how the underlying microscopic shell structure leads to the configuration changes along the yrast line and plunging Q_t values as individual configurations approach band termination.

ACKNOWLEDGMENTS

This work was supported in part by the National Science Foundation under Grants Nos. PHY-9523974 and PHY-9970991 (FSU) and in part by the U.S. Department of Energy under Contracts Nos. DE-AC05-76OR00033 (UNISOR), DE-AC05-96OR22464 (ORNL), DE-FG05-88ER40406 (WU), and DE-AC03-76SR00098 (LBNL) with Lockheed Martin Energy Research Corporation, as well as from the Swedish Natural Science Research Council, from Crafoord Foundation (Lund, Sweden) and from the Royal Swedish Academy of Sciences. F.C. acknowledges support from Colciencias (Bogotá), Contract No. 222-96. We also thank the cyclotron and GAMMASPHERE staff members at LBNL Berkeley for providing excellent research conditions.

[1] S.L. Tabor, J. Döring, G.D. Johns, R.A. Kaye, G.N. Sylvan, C.J. Gross, Y.A. Akovali, C. Baktash, D.W. Stracener, P.F. Hua, M. Korolija, D.R. LaFosse, D.G. Sarantites, F.E. Durham, I.Y. Lee, A.O. Macchiavelli, W. Rathbun, and A. Vander Molen, Phys. Rev. C **56**, 142 (1997).

[2] M. Wiedeking, R.A. Kaye, G.Z. Solomon, S.L. Tabor, J. Döring, G.D. Johns, F. Cristancho, M. Devlin, F. Lerma, D.G. Sarantites, I.Y. Lee, and A.O. Macchiavelli, Phys. Rev. C **62**, 024316 (2000).

[3] J. Döring, Y.A. Akovali, C. Baktash, F.E. Durham, C.J. Gross, P.F. Hua, G.D. Johns, M. Korolija, D.R. LaFosse, I.Y. Lee, A.O. Macchiavelli, W. Rathbun, D.G. Sarantites, D.W. Stracener, G.Z. Solomon, S.L. Tabor, A. Vander Molen, A.V. Afanasjev, and I. Ragnarsson, Phys. Rev. C **61**, 034310 (2000).

[4] A. Jungclaus, K.P. Lieb, C.J. Gross, J. Heese, D. Rudolph, D.J. Blumenthal, P. Chowdhury, P.J. Ennis, C.J. Lister, Ch. Winter, J. Eberth, S. Skoda, M.A. Bentley, W. Gelletly, and B.J. Varley, Z. Phys. A **340**, 125 (1991).

[5] B.J. Min, S. Suematsu, S. Mitarai, T. Kuroyanagi, K. Heiguchi, and M. Matsuzaki, Nucl. Phys. **A530**, 211 (1991).

[6] D. Kast, K.P. Lieb, C.J. Gross, A. Jungclaus, D. Rudolph, R. Schubart, H. Grawe, and J. Heese, Nucl. Phys. **A587**, 202 (1995).

[7] D.R. LaFosse, M. Devlin, M. Korolija, F. Lerma, D.G. Sarantites, Y.A. Akovali, C. Baktash, C.J. Gross, D.W. Stracener, J. Döring, G.D. Johns, S.L. Tabor, F.E. Durham, I.Y. Lee, A.O. Macchiavelli, and W. Rathbun, Phys. Rev. Lett. **78**, 614 (1997).

[8] M. Weiszflog, J. Billowes, J. Eberth, C.J. Gross, M.K. Kabadiyski, K.P. Lieb, T. Mylaeus, and D. Rudolph, Nucl. Phys. **A584**, 133 (1995).

[9] C. Teich, A. Jungclaus, and K.P. Lieb, Nucl. Instrum. Methods Phys. Res. A **418**, 365 (1998).

[10] A. Jungclaus, V. Fischer, D. Kast, K.P. Lieb, C. Lingk, C. Teich, C. Ender, T. Härtlein, F. Köck, D. Schwalm, J. Billowes, A. Dewald, J. Eberth, R. Peusquens, H.G. Thomas, J. Reif, M. Górska, and H. Grawe, Nuovo Cimento Soc. Ital. Fis., A **111**, 719 (1998).

[11] A. Jungclaus, C. Teich, V. Fischer, D. Kast, K.P. Lieb, C. Lingk, C. Ender, T. Härtlein, F. Köck, D. Schwalm, J. Billowes, J. Eberth, and H.G. Thomas, Phys. Rev. Lett. **80**, 2793 (1998).

[12] C. Teich, A. Jungclaus, V. Fischer, D. Kast, K.P. Lieb, C. Lingk, C. Ender, T. Härtlein, F. Köck, D. Schwalm, J. Billowes, J. Eberth, and H.G. Thomas, Phys. Rev. C **59**, 1943 (1999).

[13] D. Rudolph, K.P. Lieb, and H. Grawe, Nucl. Phys. **A597**, 298 (1996).

[14] H. Herndl and B.A. Brown, Nucl. Phys. **A627**, 35 (1997).

[15] J. Döring, G.D. Johns, R.A. Kaye, M.A. Riley, and S.L. Tabor, Phys. Rev. C **60**, 014314 (1999).

[16] D.G. Sarantites, P.F. Hua, M. Devlin, L.G. Sobotka, J. Elson, J.T. Hood, D.R. LaFosse, J.E. Sarantites, and M.R. Maier, Nucl. Instrum. Methods Phys. Res. A **381**, 418 (1996).

[17] I.Y. Lee, Nucl. Phys. **A520**, 641c (1990).

[18] H.-Q. Jin, C. Baktash, M.J. Brinkman, C.J. Gross, D.G. Sarantites, I.Y. Lee, B. Cederwall, F. Cristancho, J. Döring, F.E. Durham, P.-F. Hua, G.D. Johns, M. Korolija, D.R. LaFosse, E. Landulfo, A.O. Macchiavelli, W. Rathbun, J.X. Saladin, D.W. Stracener, S.L. Tabor, and T.R. Werner, Phys. Rev. Lett. **75**, 1471 (1995).

[19] D. Rudolph, C.J. Gross, Y.A. Akovali, C. Baktash, J. Döring, F.E. Durham, P.-F. Hua, G.D. Johns, M. Korolija, D.R. LaFosse, I.Y. Lee, A.O. Macchiavelli, W. Rathbun, D.G. Sarantites, D.W. Stracener, S.L. Tabor, A.V. Afanasjev, and I. Ragnarsson, Phys. Rev. C **54**, 117 (1996).

[20] H. Schnare, G. Winter, L. Käubler, J. Reif, R. Schwengner, J. Döring, G.D. Johns, S.L. Tabor, C.J. Gross, Y.A. Akovali, C. Baktash, D.W. Stracener, F.E. Durham, P.F. Hua, M. Korolija, D.R. LaFosse, D.G. Sarantites, I.Y. Lee, A.O. Macchiavelli, W. Rathbun, and A. Vander Mollen, Phys. Rev. C **56**, 729 (1997).

[21] K.S. Krane, R.M. Steffen, and R.M. Wheeler, Nucl. Data Tables **11**, 351 (1973).

[22] E.F. Moore, P.D. Cottle, C.J. Gross, D.M. Headly, U.J. Hüttmeier, S.L. Tabor, and W. Nazarewicz, Phys. Rev. C **38**, 696 (1988).

[23] J. F. Ziegler, J. P. Biersack, and U. Littmark, *The Stopping and Range of Ions in Matter* (Pergamon Press, New York, 1985); For SRIM version 2000.40, see www. SRIM. org

[24] I. Ragnarsson, Z. Xing, T. Bengtsson, and M.A. Riley, Phys. Scr. **34**, 651 (1986).

[25] T. Bengtsson and I. Ragnarsson, Nucl. Phys. **A436**, 14 (1985).
[26] A.V. Afanasjev, D.B. Fossan, G.J. Lane, and I. Ragnarsson, Phys. Rep. **322**, 1 (1999).
[27] A.V. Afanasjev and I. Ragnarsson, Nucl. Phys. **A591**, 387 (1995).
[28] D. Galeriu, D. Bucurescu, and M. Ivascu, J. Phys. G **12**, 329 (1986).
[29] C.E. Svensson, C. Baktash, G.C. Ball, J.A. Cameron, M. Devlin, J. Eberth, S. Flibotte, A. Galindo-Uribarri, D.S. Haslip, V.P. Janzen, D.R. LaFosse, I.Y. Lee, A.O. Macchiavelli, R.W. MacLeod, J.M. Nieminen, S.D. Paul, D.C. Radford, L.L. Riedinger, D. Rudolph, D.G. Sarantites, H.G. Thomas, J.C. Waddington, D. Ward, W. Weintraub, J.N. Wilson, A.V. Afanasjev, and I. Ragnarsson, Phys. Rev. Lett. **80**, 2558 (1998).
[30] I. Ragnarsson, V.P. Janzen, D.B. Fossan, N.C. Schmeing, and R. Wadsworth, Phys. Rev. Lett. **74**, 3935 (1995).
[31] R. Wadsworth, R.M. Clark, J.A. Cameron, D.B. Fossan, I.M. Hibbert, V.P. Janzen, R. Krücken, G.J. Lane, I.Y. Lee, A.O. Macchiavelli, C.M. Parry, J.M. Sears, J.F. Smith, A.V. Afanasjev, and I. Ragnarsson, Phys. Rev. Lett. **80**, 1174 (1998).
[32] P. Chowdhury, C.J. Lister, D. Vretenar, Ch. Winter, V.P. Janzen, H.R. Andrews, D.J. Blumenthal, B. Crowell, T. Drake, P.J. Ennis, A. Galindo-Uribarri, D. Horn, J.K. Johansson, A. Omar, S. Pilotte, D. Prévost, D. Radford, J.C. Waddington, and D. Ward, Phys. Rev. Lett. **67**, 2950 (1991).
[33] P.C. Womble, J. Döring, T. Glasmacher, J.W. Holcomb, G.D. Johns, T.D. Johnson, T.J. Petters, M.A. Riley, V.A. Wood, and S.L. Tabor, Phys. Rev. C **47**, 2546 (1993).